minerals

MDPI

Article

Rheological Properties of Aluminium Oxide Nanoparticle-Modified Cemented Paste Tailings Materials

Raouf Kaviani and Mamadou Fall *

Department of Civil Engineering, University of Ottawa, Ottawa, ON K1N 6N5, Canada; rkavi06@uottawa.ca
* Correspondence: mfall@uottawa.ca; Tel.: +1-613-562-5800 (ext. 6558)

Abstract: There is currently no research examining the rheological properties of cementitious paste backfill (CPB) materials containing aluminium oxide nanoparticles (nAlO). Knowing the yield stress and viscosity of CPB containing nAlO is crucial, especially when applying nano-CPB technology in underground mines. The purpose of this work is to thoroughly examine how nAlO affects the rheological characteristics of CPB and how those characteristics change over time. Yield stress and viscosity measurements are performed on CPB samples with different compositions (e.g., nAlO content, binder type, and superplasticizer content) at intervals of 0 min, 20 min, 1 h, 2 h, and 4 h. The study also includes measurements of the pH and zeta potential of the materials, microstructural studies (TG/DTG and XRD), and electrical conductivity (EC). The findings show that adding nAlO to CPB significantly changes its rheological properties, which in turn affects flowability. The yield stress and viscosity of CPB samples are greatly increased by the incorporation of nAlO, with the degree of influence varying based on variables including water content, curing duration, and type of binder. Because of the nAlO-induced microstructural changes in the CPB material, the interaction of nAlO and a larger fraction of nAlO, along with an increase in curing time, raises rheological characteristics and decreases paste flowability. The results of EC, DTG, and XRD, which show that binder hydration improves with nAlO dosage, corroborate this. Moreover, as nAlO content increases, the zeta potential decreases in magnitude, resulting in stronger repulsion forces and reduced flowability. However, EC, XRD, and DTG analyses suggest that the addition of 0.125% superplasticizer counteracts the flowability reduction caused by nAlO, as the superplasticizer slows down the cement hydration rate at very early curing stages. Moreover, the increase in the slag percentage from 0% to 50% and 75% of the binder content slightly decreases viscosity but greatly increases yield stress. The study's fresh perspectives contribute to the advancement of nano-CPB technology and have important ramifications for the practical use of this technology in underground mine backfill operations.

Keywords: cemented paste backfill; tailings; mine; rheology; nanoparticles; cement; aluminium oxide

check for updates

Academic Editor: Elsabe Kearsley

Received: 29 January 2025
Revised: 20 February 2025
Accepted: 24 February 2025
Published: 27 February 2025

Citation: Kaviani, R.; Fall, M. Rheological Properties of Aluminium Oxide Nanoparticle-Modified Cemented Paste Tailings Materials. *Minerals* **2025**, *15*, 246. https://doi.org/10.3390/min15030246

Copyright: © 2025 by the authors. Licensee MDPI, Basel, Switzerland. This article is an open access article distributed under the terms and conditions of the Creative Commons Attribution (CC BY) license (https://creativecommons.org/licenses/by/4.0/).

1. Introduction

In recent decades, there has been a notable increase in the usage of cemented paste backfill (CPB) material for filling mine voids. CPB, a mixture of water, binder, and tailings, is essential for improving ground control and establishing a secure working environment. It also makes it easier to properly dispose of mine waste, which lowers the danger of tailings dam collapses and tailings-induced environmental contamination and maximises resource recovery [1–6].

Ensuring the safety of persons and equipment in underground mining operations is contingent upon the stability of the subterranean CPB structure. Therefore, adequate mechanical strength must be achieved via the CPB structure. Moreover, everyone engaging in backfilling activities has the same goal of reaching CPB design strength as soon as feasible. This early strength gain is essential for prompt measures, like barricade opening and scheduling mining at the nearby stope, which will ultimately shorten the mining cycle and increase overall profitability and productivity [7–13].

Nevertheless, the binder, water, and tailings—traditional CPB production ingredients—are not naturally made to encourage a quick increase in CPB strength in the early stages of the process. Ordinary Portland cement (OPC) is still typically the most widely utilised binder in the manufacture of CPB. In addition to raising costs, using ordinary Portland cement (OPC) as a binding agent in CPB slows down the rate at which the material gains strength in its early stages. Furthermore, a significant amount of greenhouse gases is released during the manufacture of OPCs. At about 4 billion tonnes per year, the present rate of production accounts for 7% of the world's CO_2 emissions [7]. The mining industry's growing focus on sustainability makes the overuse of OPC in CPB technology incompatible with this goal.

Supplementary cementitious materials (SCMs), most notably blast furnace slag (BFS), have been utilised regularly to partially substitute standard OPC in CPBs due to cost concerns. The disadvantage of this approach is that slag has a slower rate of early hydration, which causes a discernible decline in early-age strength and the pace of strength growth in CPBs that contain slag. Despite this, the procedure helps reduce costs and the carbon footprint associated with CPBs. Mine productivity is being challenged by this slowdown. In response, silica fume (SF), a highly reactive pozzolanic material widely used in conventional cementitious systems [11], has been proposed as a partial OPC replacement in CPBs to enhance mechanical properties and durability [3]. However, its incorporation significantly impacts rheology by increasing initial yield stress and structural buildup over resting time due to its ultrafine particle size and high surface area [3]. Structural buildup, or the gradual increase in static yield stress over resting time, is critical for CPB transportability and placement in underground mines. A higher structural buildup rate can enhance early strength gain but may also increase pipeline pressure requirements during pumping. Increased yield stress and viscosity can make CPB pumping and placement more challenging, potentially leading to pipeline blockages with substantial financial consequences. As a result, the mining industry continues to explore alternative strategies to accelerate CPB strength development while minimizing its environmental impact. As a result, the mining industry continues to explore alternative strategies to accelerate CPB strength development while minimising its carbon imprint impact [8,9].

One new development in CPB technology is the addition of nanoparticles, namely Aluminium Oxide nanoparticles (nAlO), as additives. By adding Al_2O_3 nanoparticles to the CPB mixes while lowering the OPC content, this novel method seeks to improve the mechanical performance and lessen the carbon footprint of CPBs [2]. The effective use of nanoparticles in the production of high-performance concrete with enhanced early-age strength and strength enhancement rates [14–20] is the inspiration for this development. Recently, there has been a lot of interest in the use of nanoparticles in cement-based materials (CBMs), such as concrete. Research has shown that adding nanoparticles can significantly improve the mechanical characteristics of traditional mortar or concrete materials because of their chemical and physical effects (such as filler effect and enhanced cement hydration). In particular, nano-Al_2O_3 has been studied in great detail when it comes to CBMs. Within the field of building materials, and specifically within the framework of cement and concrete research, a great deal of study has demonstrated the effectiveness of adding

nano-Aluminium Oxide (nAlO) particles. These investigations have demonstrated that the addition of these nanoparticles to the mixes of concrete or mortar can significantly improve their strength and strength gain rate (e.g., refs. [21–28]). Because of its filler function, aluminium oxide helps to reduce porosity, which promotes the development of a denser cementitious matrix.

Beyond the necessary emphasis on strength, the fresh material's flowability or transportability is another crucial design factor in the context of CPB. To enable efficient pumping and delivery to mine cavities, it is imperative to provide an appropriate flow capability (stopes). Inadequate flow ability can result in issues like clogs in pipes, which can cause serious financial losses for mining companies (e.g., refs. [10,12,13,29–32]). Regretfully, nothing is known about the specific effect of nAlO particles on CPB's ability to flow. In order to assess flow ability, one usually looks at the rheological characteristics of CPB, specifically looking at its viscosity and yield stress, which indicate the material's resistance to deformation and flow initiation, respectively [33,34].

However, a number of fundamental questions concerning the interaction between nAlO and the rheological characteristics of CPB remain open. These include questions about how nAlO affects the yield stress of CPB, how it affects the viscosity of fresh CPB, how these variables change during the curing and transport stages, how nAlO leads to changes in the microstructure of CPB, and how these factors may interact with superplasticizers or inorganic admixtures such as slag. Filling these important knowledge gaps is essential to the successful integration and use of nano-CPB technology. In order to provide important information on the effects of nAlO particles on the rheological, microstructural, and chemical properties of CPB for different types of binders, with or without superplasticizers, over varying periods of time, this study employs a variety of experimental methodologies, including extensive rheological testing, microstructural analysis, chemical evaluation and an extensive monitoring program.

2. Experimental Approach

2.1. Specimen Preparation and Materials

2.1.1. Tailings

In order to ensure the reliability of the results, the study used synthetic silica tailings (ST), which are distinguished by their non-reactive and non-acid-producing features. Quartz minerals make up the majority of ST, which is similar to the mineral makeup of natural tailings from several hard rock mines in Canada. The grain size distribution of the medium-sized ST was comparable to that of the tailings from other mines in eastern Canada (see Figure 1 and Table 1).

Table 1. Physical characteristics of the tailings used.

Element	Gs	D_{10} (μm)	D_{30} (μm)	D_{50} (μm)	D_{60} (μm)	Ss (cm^2/g)
ST	2.7	1.9	9.0	22.5	31.5	3600
An average of 9 mines	–	1.8	9.1	20.0	30.8	–

Gs: specific gravity; Ss: specific surface area; ST: synthetic silica tailings.

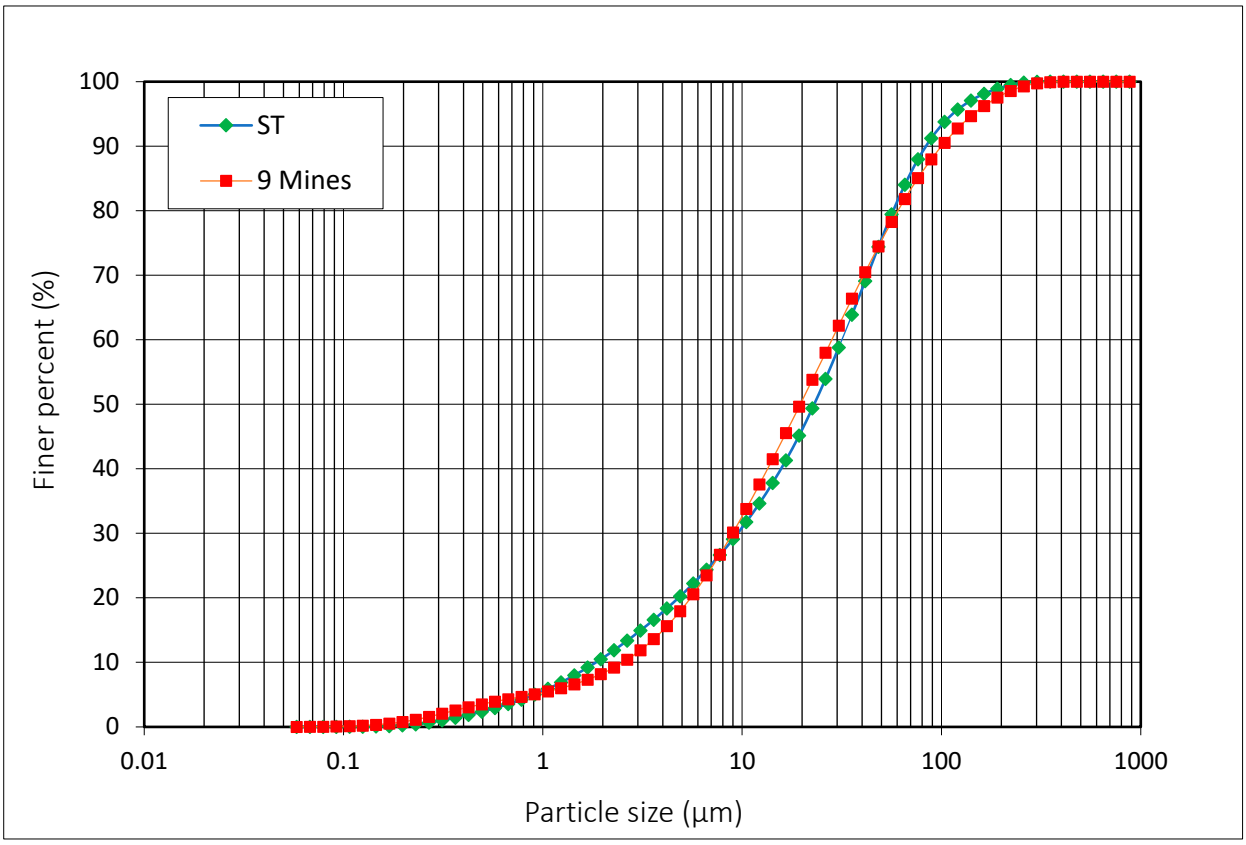


Figure 1. Distribution of silica tailings (ST) grain sizes and average grain sizes of tailings from nine Eastern Canadian mines.

2.1.2. Binders and Water

The main binder was regular PC type I (PCI), which has a specific gravity of 3.2. Furthermore, as is customary in Canadian CPB plants, a mixture of PC and slag was used to prepare a few CPB specimens at a 50/50 and 25/75 weight ratio, with a binder component of 4.5% by weight [12,26]. Table 2 lists the binders' chemical makeup and physical characteristics, which were mostly ascertained by X-ray fluorescence (XRF). Distilled water was used to prepare all of the backfill samples, with a water-to-cement ratio of 7.8.

Table 2. Primary chemical and physical properties of the Portland cement and slag used.

	Na_2O	MgO	Al_2O_3	SiO_2	K_2O	CaO	TiO_2	MnO	Fe_2O_3	Relative Density	Specific Surface Area (cm^2/g)
PCI	0.34	2.58	4.81	20.38	0.96	62.70	0.23	0.05	3.61	3.2	1300
Slag	0.28	11.78	10.60	35.57	0.48	39.21	0.47	0.30	0.62	2.8	2100

2.1.3. Nano-Aluminium Oxide

Sourced in colloidal form from Dow Corning, Inc. (Midland, Michigan, USA), nano-Aluminium Oxide (nAlO) is an amorphous Al_2O_3 with a high specific surface area and purity. It is used at several concentrations—0%, 1%, and 3% by total mass of binder materials. The chemical and physical properties of the used nAlO particles are displayed in Table 3.

Table 3. Characteristics of the Nano-Al_2O_3 (NA) nanoparticles used.

Form	Nanopowder
Particle size	<50 nm (TEM)
Surface area	>40 m^2/g (BET)
Molecular Weight	101.96
Colour	White

Data obtained from suppliers.

2.1.4. Superplasticizer

A superplasticizer supplement was added to some CPB samples (0.125% by weight of the mixture). The chosen superplasticizer was BASF's Master Glenium 7500 (Master G), which satisfies ASTM requirements for high-range water-reducing admixtures [35,36].

2.2. Specimen Preparation

Different CPB combinations with varying amounts of nAlO were created in addition to reference (control) samples that had no nAlO (0% nAlO). For five minutes, the dry materials were well blended using a mechanical mixer while maintaining a constant water-to-binder ratio (W/B) of 7.8 and a binder content of 4.5 weight percent. After adding the water and nAlO, the mixture was stirred for an additional five minutes. The CPB was then placed into plastic cylinders measuring 10 cm in height and 5 cm in diameter; bigger cylinders measuring 10 cm in diameter and 20 cm in height were utilised for monitoring. The CPB cylinders were manually vibrated to release any trapped air, and then they were sealed and allowed to cure at ambient temperature for predetermined amounts of time to replicate different backfill transport times. Table 4 lists the mix proportions for the prepared CPBs. Additionally, a constant W/B ratio of 1 was used to make cement paste samples for microstructure investigation. Following curing, the CPB and CP specimens underwent a number of tests and analyses (Table 5).

Table 4. Mix composition of the specimens prepared for rheological tests.

Sample Name	Nano-Al_2O_3 [(a)] (%)	Binder (%)	Binder Type	w/b	Superplasticizer (%)
CPB-PCI-0%nAlO	0	4.5	PCI	7.8	0
CPB-PCI-1%nAlO	1	4.5	PCI	7.8	0
CPB-PCI-3%nAlO	3	4.5	PCI	7.8	0
CPB-PCI 1%nAlO-SP	1	4.5	PCI	7.8	0.125
CPB-PCI 3%nAlO-SP	3	4.5	PCI	7.8	0.125
CPB-50%PCI/50%Slag 0%nAlO	0	4.5	PCI/Slag (50/50) [(b)]	7.8	0
CPB-50%PCI/50%Slag 1%nAlO	1	4.5	PCI/Slag (50/50)	7.8	0
CPB-50%PCI/50%Slag 3%nAlO	3	4.5	PCI/Slag (50/50)	7.8	0
CPB-25%PCI/75%Slag 0%nAlO	0	4.5	PCI/Slag (25/75)	7.8	0
CPB-25%PCI/75%Slag 1%nAlOCPB	1	4.5	PCI/Slag (25/75)	7.8	0
CPB-25%PCI/75%Slag 3%nAlOCPB	3	4.5	PCI/Slag (25/75)	7.8	0

[(a)] by the mass of the binder; [(b)] PC/Slag (50/50) = the blend weight ratio of Portland cement to slag is 50/50.

Table 5. Summary of the mix composition of the specimens prepared for XRD, TG/DTG analyses.

Sample Nomenclature	Binder Content (%)	PCI in the Binder (%)	Slag in the Binder (%)	SP (%)	Tailing Type	$\frac{W}{C}$ Ratio	Mixing Water	Nanop Content (%)	Nanop Type	Curing Time (h)
CPB-PCI 0	-	100	0	0	none	1	DW	0	none	2
CPB-PCI 1	-	100	0	0	none	1	DW	1	nAlO	2
CPB-PCI 3	-	100	0	0	none	1	DW	3	nAlO	2
CPB-PCI/Slag 3	-	50	50	0	none	1	DW	3	nAlO	2
CPB-PCI 3-SP	-	100	0	0.125	none	1	DW	3	nAlO	2

DW: distilled water; SP: superplasticizer; Nanop: nanoparticles.

2.3. Methods of Testing and Analysis

2.3.1. Viscosity Test

A digital viscometer (Model DVE; Brookfield Engineering Laboratories Inc., Middleboro, MA, USA) with an immersed spinning spindle was used to measure the viscosity of the backfill specimen. Viscosity can be measured instantly with this device since it uses a calibrated spring to rotate a spindle at a steady speed. A rotary transducer's spring deflection is what determines the mixture's viscous drag [37]. Additional information on CPB viscosity measurements with this viscometer is given in [36]. Samples were evaluated at specified curing times of 0 min, 20 min, 1 h, 2 h, and 4 h. To guarantee the reproducibility of results, tests were repeated at least twice.

2.3.2. Vane Shear Test

To determine the samples' yield stress, the vane shear test was used. The study used a vane device called a Wykeham Farrance (Model 23500), which is made up of a four-blade vane and a motor that rotates the vane through a calibrated torsion spring at a steady rate of 0.18 rpm. Vane shear tests were conducted in accordance with the ASTM D4648/D468M-13 standard at 0 min, 20 min, 1 h, 2 h, and 4 h post-mixing. The 2.5 cm × 2.5 cm four-bladed vane was carefully inserted into the sample's centre to minimize container-induced disturbances. After full insertion, the sample was left to stabilise for 30 s to reduce insertion effects. To guarantee homogeneity and replicate the continuous shear experienced by the CPB during transit, the sample was physically stirred and then mixed with a spoon for one minute prior to each test. This prevented any settling of the tailing grains owing to self-weight. After positioning the vane at the centre of the specimen's surface, the apparatus was activated. The vane was rotated at a uniform speed to minimise the effects of factors such as viscous drag, instrument inertia, and inadequate damping. The torque head recorded the torsional moment, and the peak torque value was identified. After noting the highest torque, the yield stress associated with it was computed using Equation (1) (ASTM D4648 [38]):

$$\tau_y = \frac{2T_m}{\pi D^3 \left[\frac{1}{3} + \frac{H}{D}\right]} \quad (1)$$

where H is the vane's length, D is its diameter, T_m is the maximum torque that has been established, and τ is the yield stress.

To ensure the accuracy of the findings, every test was carried out a minimum of three times.

2.3.3. Microstructural Analysis

For CPB specimens with and without nAlO, XRD, thermal gravimetry (TG), and differential thermal gravimetry (DTG) investigations were conducted on CPB cement

pastes to clarify the microstructural alterations. After four days of drying at 45 °C to eliminate any remaining water, cement paste specimens were ground into a powder. XRD and TG/DTG tests were used to ascertain the hydration products' phase composition. Using a thermal analyser (TGA Q5000 V3.15 Build 263), TG/DTG analysis was carried out by heating the specimens at a rate of 10 °C/min from 0 to 1000 °C in a nitrogen environment. A Rigaku Ultima-IV diffractometer, running at 40 kV and 44 mA, was used to do the XRD analysis. It was programmed to scan at a rate of 0.5°/min with an increment of 0.02 from 2° to 80° of the 2θ range.

2.3.4. pH and Zeta Potential (ZP) Measurements

With an accuracy of ±0.003, the pH values of the backfill specimens were ascertained using Metrohm 704 (Metrohm AG, Herisau, Switzerland). To validate the results, each measurement was made at least twice, and the average values were noted. The Zetasizer Nano series was used to perform zeta potential measurements, which offer insights into particle-particle interactions at the microscale [10]. The phase analysis light scattering method was utilised to quantify the electrophoretic mobility of particles in suspension (PALS). The Henry Equation was used to calculate ZP [39]. Distilled water was used to prepare the specimens, and for reproducibility, each ZP measurement was performed five times.

2.3.5. Electrical Conductivity Monitoring

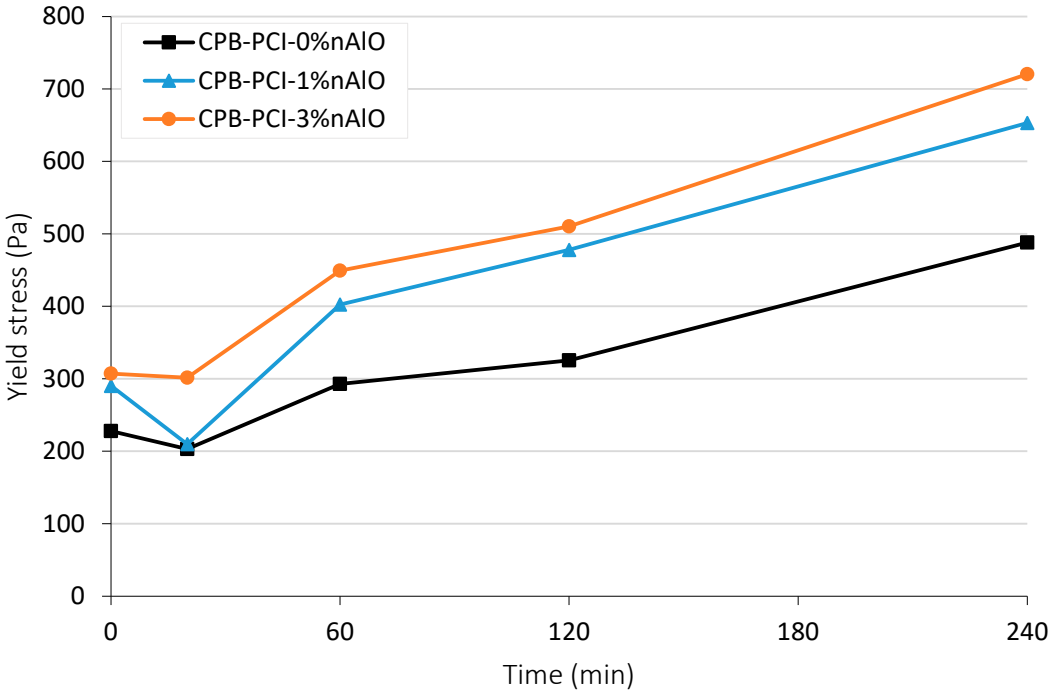
Changes in electrical conductivity (EC) can be linked to variations in the quantity and/or mobility of charge-carrying ions and can therefore serve as a reliable indicator of the degree of cement hydration reaction [36,40]. Additionally, EC measurements are useful for monitoring the structural transformations that take place in hydrating cementitious systems e.g, [36,40]. The EC value of cement-based materials is affected by the concentration of ions within the pore network [11]. As hydration progresses, capillary pores in the hardening cement paste gradually become filled with hydration products, leading to the development of a solid microstructure and an increase in mechanical strength [11]. Consequently, the electrical conductivity of cement paste decreases over time [36]. For this research, an EC sensor (5TE electrical conductivity) from Decagon Devices, Inc. was utilised to obtain an additional understanding of the cement or binder reaction processes influencing the rheological characteristics of CPB with different nAlO levels. By putting an alternating current between two electrodes and measuring the resistance between them, the sensor—which was placed in the centre of each specimen—measured the electrical conductivity of the backfill specimens. Data from the sensor was gathered using a data recorder.

3. Results and Discussion

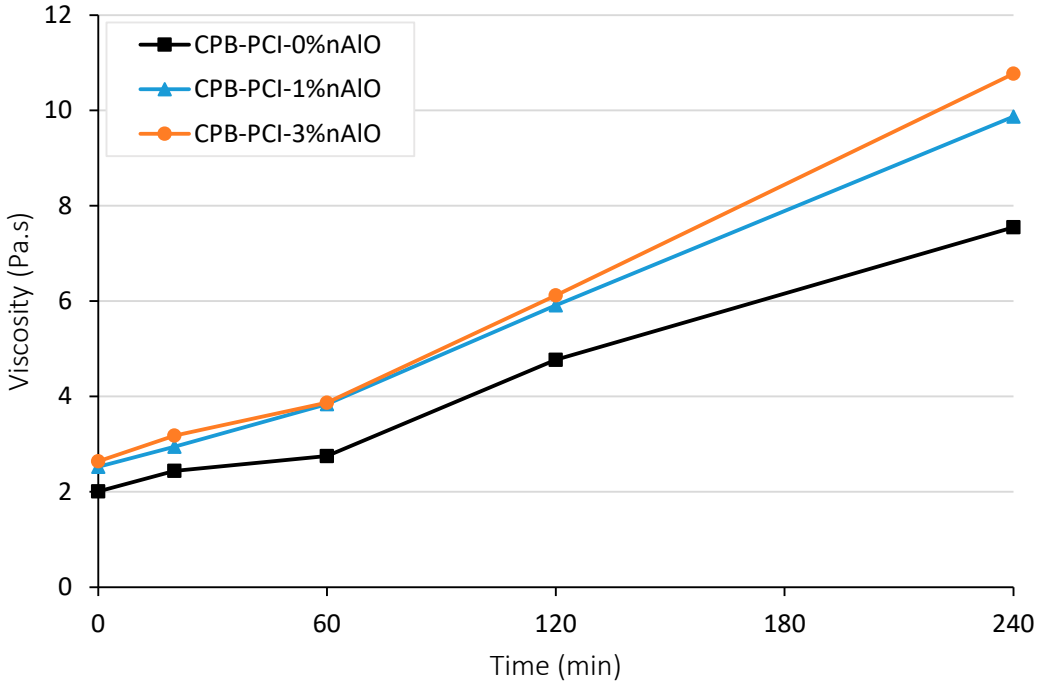
3.1. Influence of Nano-Aluminium Oxide (nAlO) on the Rheological Properties of CPB Made of Portland Cement

Figure 2 shows how nAlO affects the time-dependent alterations in the yield stress and viscosity of CPB with 100% Portland cement acting as the binder. This figure shows that the yield stress and viscosity of the backfill grow with curing time, regardless of the amount of nanoparticles present. This behaviour results from the way cement hydration changes with time. As the hydration reaction progresses, more cement hydration products, such as C-S-H, ettringite, and CH, are produced [40,41]. This increases the material's yield stresses and inter-frictional resistance by encouraging the aggregation of particles and the formation of more cohesive structures [10,12]. Furthermore, the size of hydration products also increases in tandem with the increasing degree of cement hydration [13,40,42]. As a result, the viscosity of CPB samples increases gradually as the solid volume percentage

grows steadily [16,41,43]. In addition, the process of cement hydration uses up free water, which causes the water film around the particles to get thinner. A progressive increase in yield stress is directly related to this decrease in water content. It is evident that this drop in water content is correlated with an increase in the CPB's solid volume portion. Increased solid volume fractions lead to increased particle-particle interactions, which in turn raise the apparent viscosities of fresh CPB samples (refs. [13,17]).



(**a**)



(**b**)

Figure 2. Effect of nano-Al_2O_3 (nAlO) content on the evolution of the rheological properties of CPB with Portland cement: (**a**) yield stress; (**b**) viscosity.

The assertion that longer curing times lead to the production of more cement hydration products is supported by experimental results from thermal analyses (TG/DTG), as shown by Figure 3's representation of TG/DTG studies conducted on cement pastes cured for 60 and 240 min. Three separate endothermic peaks, or weight losses, may be seen in this image for temperature ranges of 50–200 °C, 400–450 °C, and 600–700 °C. The principal causes of weight loss between 50 and 200 °C are the dehydration of hydration products such as gypsum, C-S-H, carboaluminates, and ettringite, as well as the evaporation of bound water. The breakdown of calcite ($CaCO_3$) is responsible for the peak between 600 °C and 700 °C, while the dehydroxylation of CH is primarily responsible for the peak between 400 °C and 450 °C (refs. [44–48]). Figure 3 clearly shows that the specimen cured for 60 min has a lower peak in temperature ranges of 50–200 °C and 400–450 °C than the cement paste cured for 240 min. This data suggests that the CPB samples with extended curing times produced more hydration products.

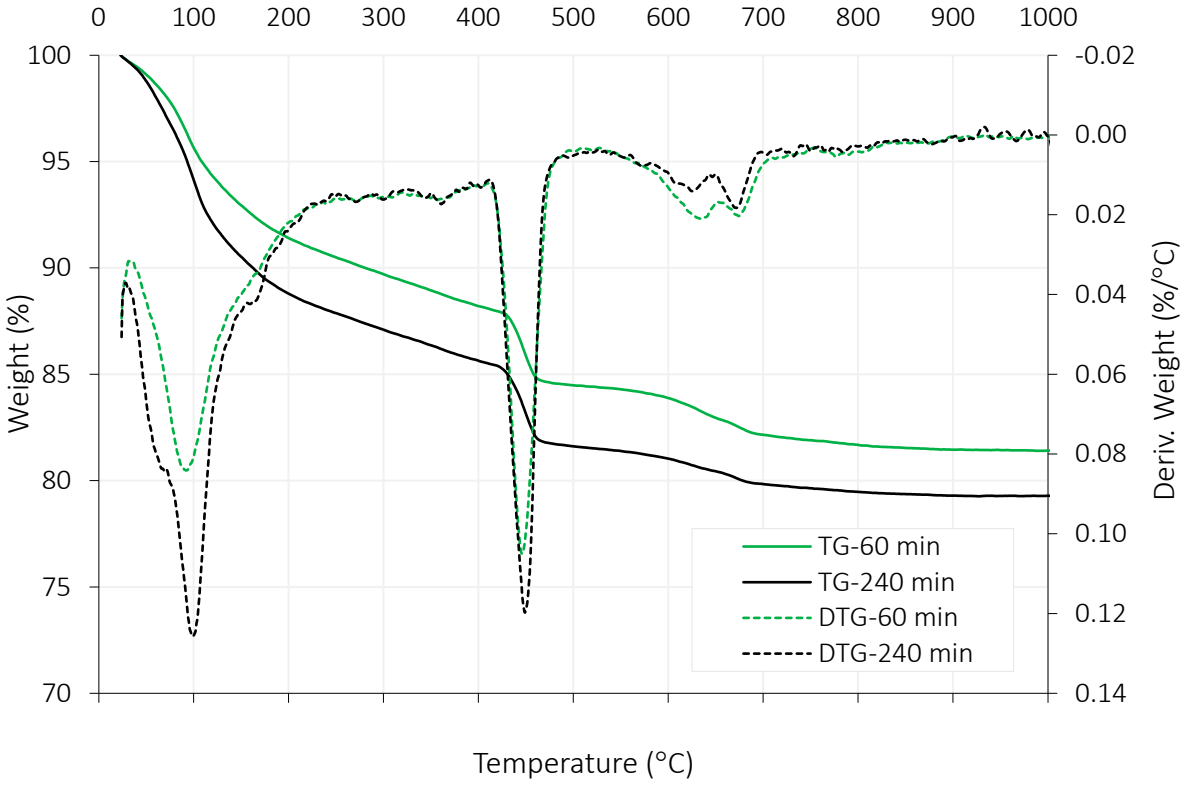


Figure 3. TG/DTG analysis results of cement paste samples without nAlO and cured for 60 min and 240 min.

Furthermore, Figure 2 shows that the inclusion of nanoparticles significantly altered CPB's flow ability. Regardless of the testing age, it demonstrates a significant increase in backfill yield stress and viscosity with the addition of nAlO. The yield stress of the specimen containing 3% nAlO, for example, was 307 Pa, 301 Pa, 449 Pa, 510 Pa, and 720 Pa at 0 min, 20 min, 1 h, 2 h, and 4 h, respectively. This represents an increase of approximately 35%, 44%, 53%, 57%, and 47% compared to the 0% nanoparticle sample. In comparison to the 0% nanoparticle samples at 0 min, 20 min, 1 h, 2 h, and 4 h, respectively, the yield stress of samples containing 1% nAlO increased by roughly 27%, 3%, 37%, 46%, and 33%. Furthermore, compared to the control sample, the addition of 1% and 3% nAlO increased the viscosity at 4 h by 31% and 43%, respectively. Moreover, the addition of 3% nAlO had a stronger effect on CPB viscosity at 0 h and 20 min compared to 1%. A number of variables working together can be responsible for the flowability loss observed in the presence of

nAlO, as evidenced by higher yield stress and viscosity. The filler effect that nanoparticles exert, the enhancement of cement hydration caused by nAlO, the increased water demand brought on by the presence of nanoparticles, and the greater flocculation or agglomeration of the paste as a result of nAlO particles are some of these factors [40,49–56]. Below is a more detailed discussion of these factors, which together are responsible for the change in rheological properties of CPB in the presence of nAlO.

- nAlO filler effect: It is well known that nanoparticles are effective in partially filling the empty spaces in a cementitious material, which causes the microstructure to become denser [42]. This finally increases the yield stress and viscosity of the backfill material by increasing the frictional resistance between the particles and the solid volume fraction in the CPB material (ref. [18,40]).
- Enhancement of the cement hydration by nAlO: The extremely small dimensions of nAlO particles (see Table 3) provide an extensive number of nucleation sites, helping the formation of numerous hydration products, notably C-S-H. These nucleation sites play an essential role in enhancing and intensifying the hydration process of essential cement compounds. The sample containing nAlO has a greater amount of hydration products, according to the XRD data (Figure 4). For instance, the sample containing nAlO has a greater CH intensity than the one containing no nAlO. In fact, the sample with nanoparticles (nAlO) had a greater CH intensity at 18 and 34° 2-theta than the sample without nAlO. This observation highlights the effect of nAlO on cement hydration by implying a higher production of CH in specimens with that addition. This conclusion about the inclusion of nAlO particles producing additional hydration products is also consistent with the findings of TG/DTG studies performed on cement pastes that were 2 h old and had varying nAlO concentrations (0%, 1%, and 3%), as shown in Figure 5. According to these findings, the cement paste that has been treated with nAlO shows the strongest endothermic peaks and weight loss between 100° and 180 °C. These indicators point to a higher yield stress and viscosity level due to an enhanced production of hydration products. The agreement with the results of the EC monitoring of CPB samples with different percentages of nAlO, shown in Figure 6, gives further support to this explanation. This graph shows that the curves initially show increasing tendencies, which can be attributed to the cement's breakdown phase. Aluminate, potassium, calcium aluminium oxide ions, and other types of ions were released when water was added to the cement, causing the cement's ions to dissolve. The paste's electrical conductivity was improved by these liberated and mobile ions [57,58]. CH, C-S-H, and ettringite were among the hydrates that filled the capillary holes as another hydration reaction occurred. As a result, EC decreased as a result of the decline in ion mobility and concentration [59]. As shown in Figure 6, the EC for the nAlO-containing samples was higher than that of the nAlO-free samples during the early stage (up to 2 h or 120 min). Furthermore, the addition of nAlO resulted in a noticeable shift of the EC peaks to shorter hydration periods, indicating faster hydration reaction rates. In fact, the specimens containing 3%, 1%, and 0% nAlO had conductivity peaks at 3.7 h (200 min), 3.6 h (220 min), and 4.0 h (240 min), respectively. This also aligns with the observation that the slopes of the 3%-nAlO and 1%-nAlO samples prior to the EC peak were steeper than those of the control sample, suggesting an acceleration in cement hydration within the chloride-containing samples. In fact, the slope preceding the EC curve's peak correlates with the rate of the hydration reaction; a sharper slope signifies a quicker hydration process [50]. This early-stage fast acceleration of cement hydration is consistent with yield stress and viscosity observations shown in Figure 2.

- nAlO-induced increase in water demand: The water requirement of the CPB mixture to attain appropriate flowability was directly impacted by the addition of nAlO to the CPB. The well-established fact is that nanoparticles raise the need for water [60,61]. Because of the nanoparticles' large surface area (>40 m^2/g), which adsorbs free water on their surface, there is a higher water demand when they are present. Greater surface area to be wetted results from finer particles. As a result, more water is needed to keep the CPB's workability or flowability at a respectable level [62].
- Enhanced flocculation or agglomeration of the paste owing to nAlO particles: The tendency for flocculation or agglomeration after adding nAlO particles is consistent with the results of zeta potential (ZP) measurements made on the CPBs with different concentrations of nAlO particles (Figure 7). Higher ZP magnitudes are linked to stronger electrostatic repulsion between charged particles, which leads to improved dispersion. ZP determination is a technique used to evaluate the surface charge and potential stability of suspended particles. The electrostatic surface charge, or ZP, determines how much repulsion or attraction there is between colloidal particles [57]. As a result, ZP may be used to identify the nAlO particle dispersal process in the alkaline Portland cement paste environment (Figure 7). The pH trend over time for PCI-CPB samples containing 0% and 3% nAlO is shown in Figure 8. In all CPB samples, the creation of $Ca(OH)_2$ as a result of cement hydration creates an alkaline state (high pH). The pH values of the specimens containing 0% and 3% nAlO were 12.79 and 12.97, respectively, following a 25-min curing period. Moreover, pH levels rose to 13.03 and 13.08 for samples containing 0% and 3% nAlO, respectively, after two hours of ageing. Figure 8 shows that the pH of CPB with 3% nAlO is higher than the pH of CPB without nAlO. This is consistent with the theory that nAlO particles improve cement compound hydration, which releases more alkali ions into CPB pore water and raises pH. The ZP measurement findings for CPB with 100% PCI, including 1% and 3% nAlO, are shown in Figure 7 beside the control sample. When the nAlO % rises, the ZP of the CPB falls, suggesting that there is a stronger electronic double-layer repulsive force when nAlO is absent. Altered rheology and increased water demand are caused by reduced repulsion and low ZP, which is congruent with the outcomes of yield stress and viscosity, as was previously discussed [14].

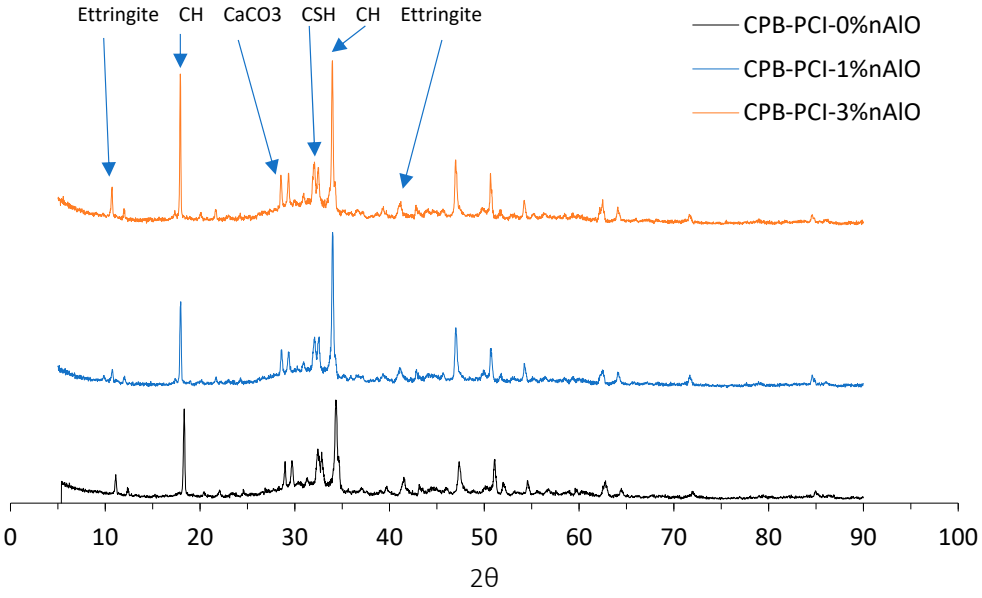


Figure 4. XRD results of cement paste of PCI-CPB with 0%, 1%, and 3% age of nAlO inclusion after 2 h.

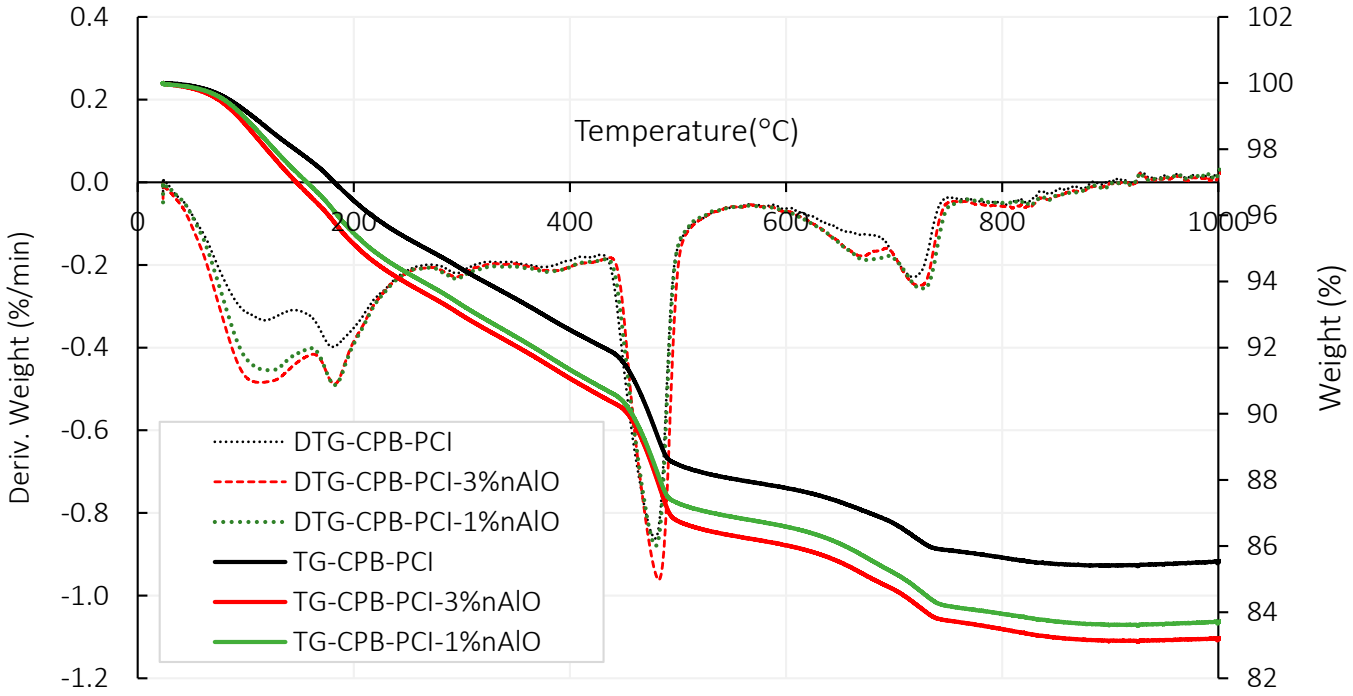


Figure 5. TG/DTG diagrams for cement pastes with 100% PCI cured for 2 h and containing 0%, 1%, and 3% of nAlO particles.

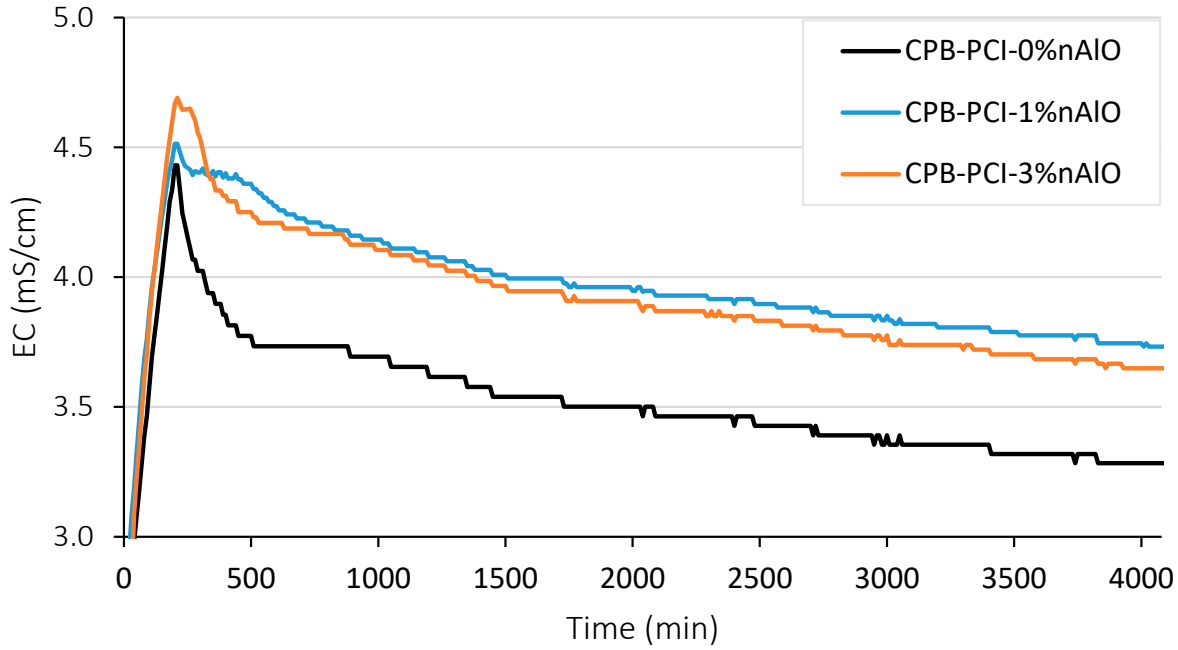


Figure 6. Changes in electrical conductivity of PCI-CPB specimens.

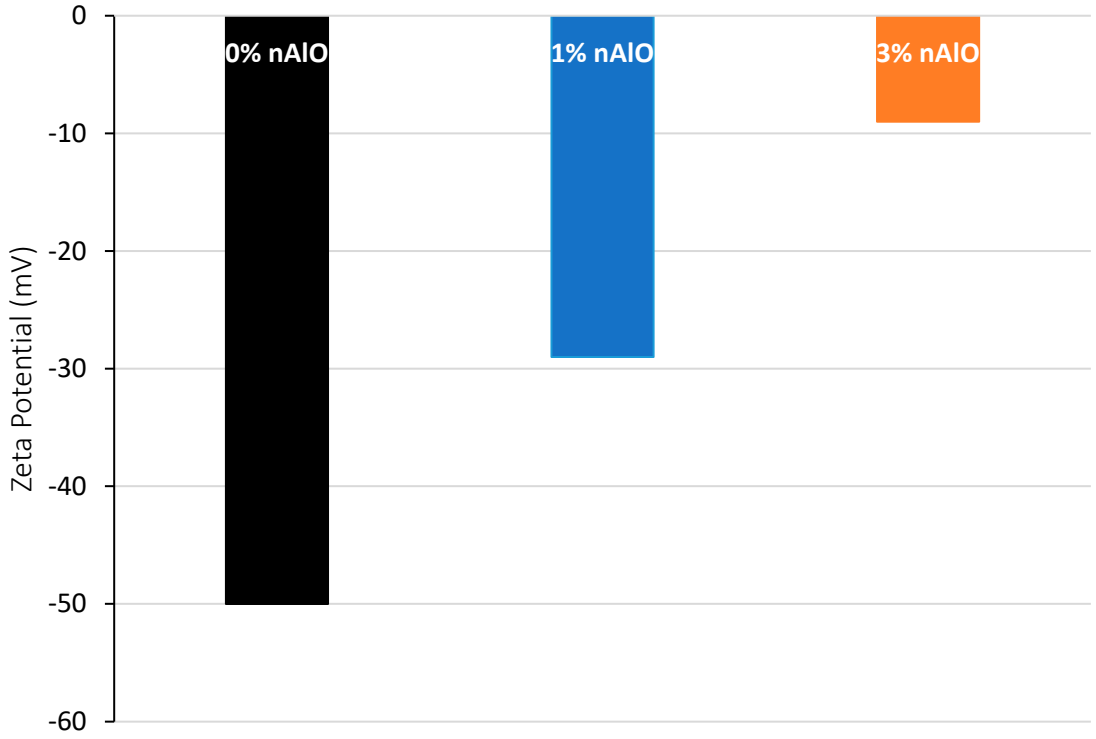


Figure 7. Zeta potentials of 2 h old CPB with 0% nAlO vs. 1% nAlO vs. 3% nAlO.

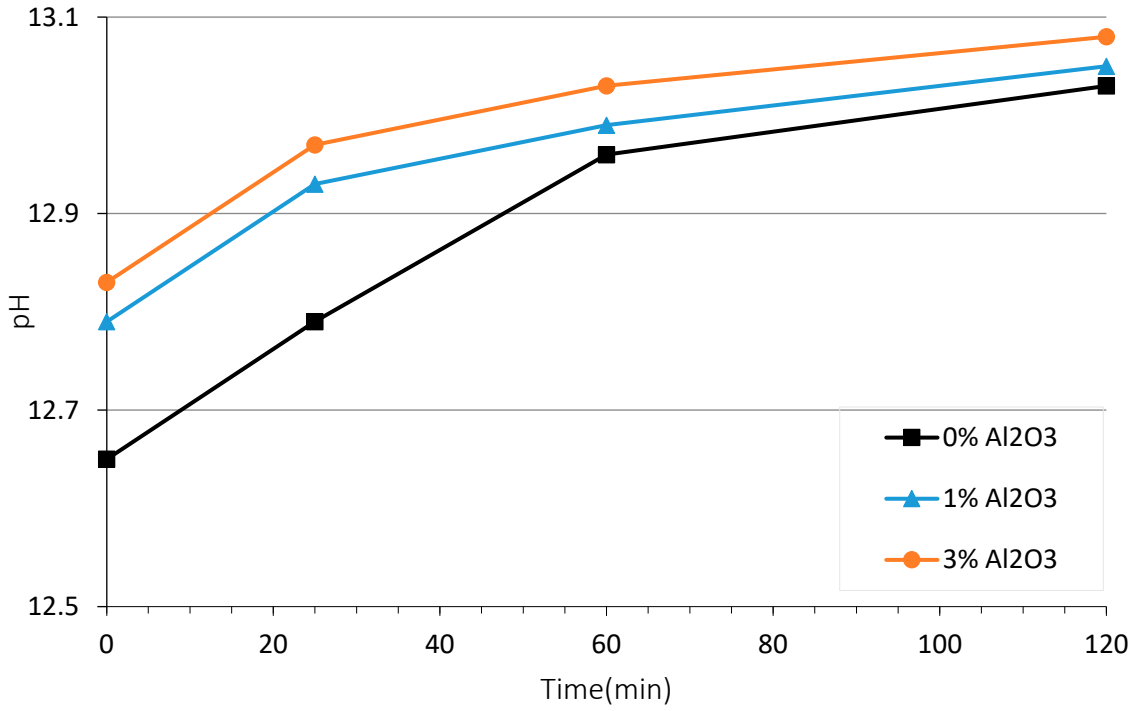


Figure 8. pH evolution of CPBs with 0% nAlO vs. 1% nAlO vs. 3% nAlO.

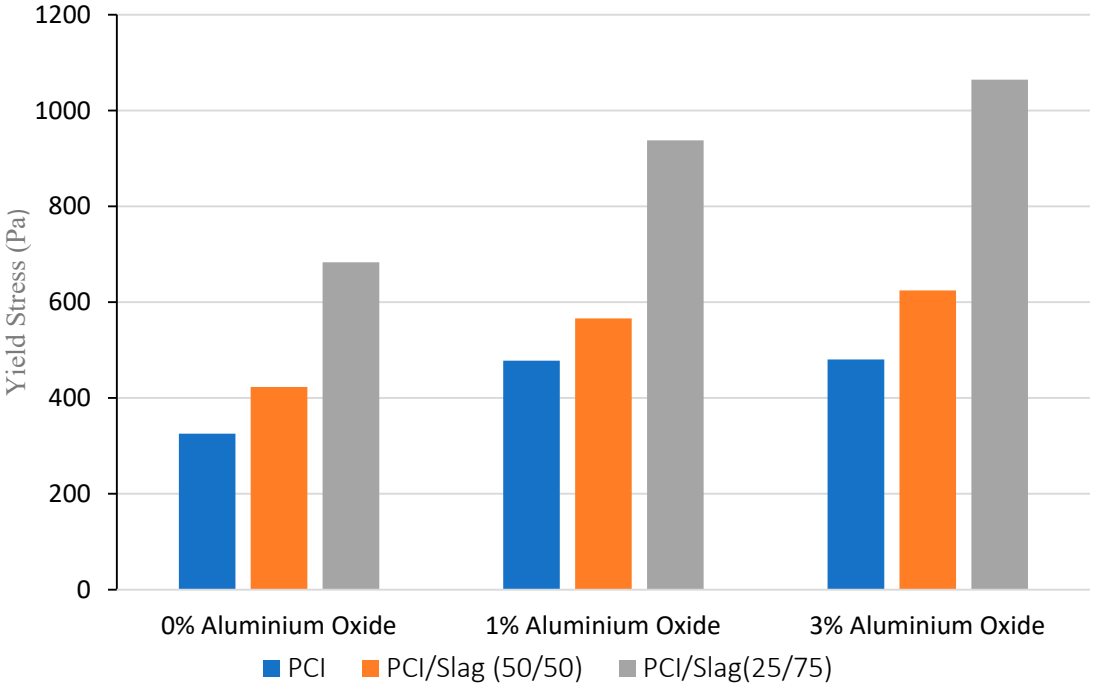
3.2. Influence of Nano-Aluminium Oxide (nAlO) on the Rheological Properties of CPB with Slag

Cement and mineral mixtures, like slag, have been combined and used extensively in cemented backfill in recent years. CPB is less expensive and more durable when blended cement is used [41]. Furthermore, using slag—a low-carbon binder—helps a mine lower its carbon footprint, supporting sustainable mining practices and the handling of mine waste. Therefore, additional testing was done to evaluate the rheological properties of backfill in which slag was used in place of some of the Portland cement. Three different replacement

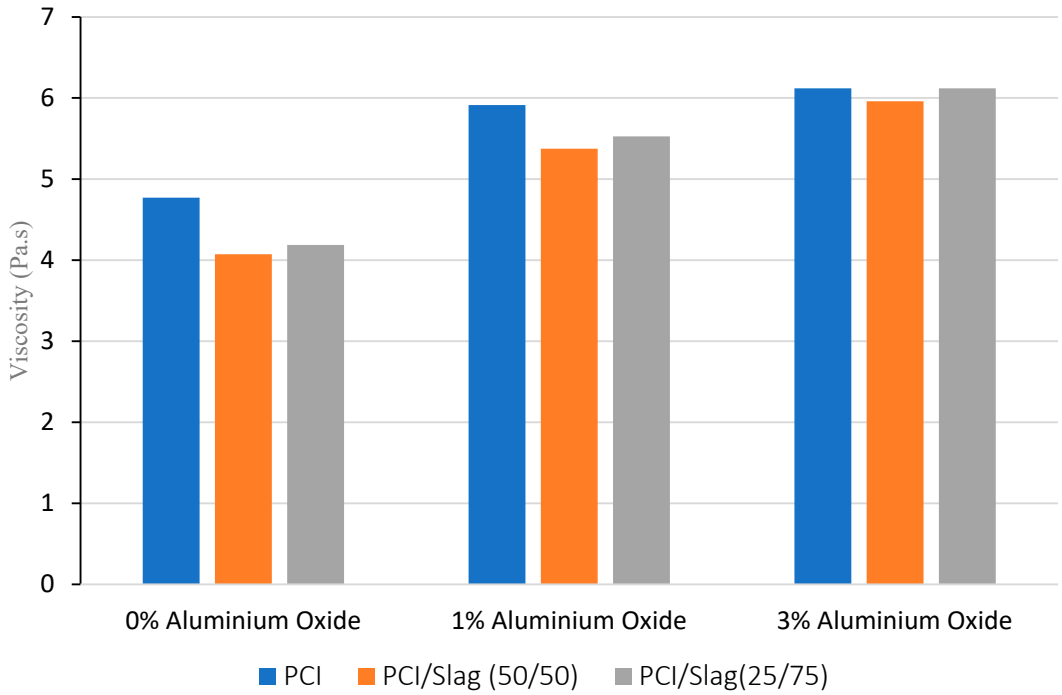
scenarios were investigated: a replacement of 0% represented as PCI, a replacement of 50% represented as PCI/Slags (50/50), and a replacement of 75% represented as PCI/Slags (25/75).

Following a 2-h curing period, Figure 9 shows the effects of different nAlO percentages on the yield stress (Figure 9a) and viscosity (Figure 9b) of backfill samples with PCI, PCI/Slag (50/50), and PCI/Slag (25/75). A consistent tendency can be seen in the data: independent of the binder used, yield stress and viscosity demonstrate an ascending trend with increasing nAlO content and curing time across all sample types—PCI, PCI/Slag (50/50), and PCI/Slag (25/75). The section that came before this one explained the underlying mechanisms that cause this behaviour. Specifically, Figure 9a shows that samples incorporating slag consistently show higher yield stress than ones containing PC alone, whether or not nanoparticles are present. Additionally, there is a positive association between the yield stress and the amount of slag in the mixture. For example, during a 2-h ageing period without nAlO, the yield stress values for samples with 100% PCI, PCI/Slag (50/50), and PCI/Slag (25/75) were 325, 423, and 683 Pa, respectively. Changes in inter-particle forces resulting from the partial substitution of PCI with slag can explain the increased yield stress found in samples containing PCI/Slag. Van der Waals attraction and electrostatic repelling forces affect a suspension's coagulation and dispersion behaviour. Aggregates form when particle attraction dominates, leading to an increase in yield stress. Figure 10 presents the zeta potential analysis results for fresh CPB samples with varying PCI/slag replacement ratios (excluding nAlO). Notably, the Slag-CPB samples exhibit lower absolute zeta potential values (25 mV for PCI/Slag (50/50) and 20 mV for PCI/Slag (25/75)) compared to the 100% PCI-CPB sample (50 mV). This indicates a reduced electrical double-layer repulsion force in the slag-containing samples. Consequently, CPBs with slag particles exhibit greater interparticle attraction, which contributes to higher yield stress. Furthermore, the lower zeta potential in Slag-CPB, consistent with DLVO theory, implies the possible creation of a "secondary minimum", which is typified by a weaker and perhaps reversible adhesion between particles. For the vane blade to create flow in the suspension, more external force must be provided for these weak flocs to maintain their stability during Brownian motion [19,20]. Furthermore, it is clear from Figure 9b that, whether or not nanoparticles are present, the viscosity of the CPB shows a different pattern from the yield stress with the introduction of Slag into the binder system. Stated differently, the viscosity of the backfill samples is decreased upon the addition of slag as a partial replacement for PC. There are two fundamental reasons that explain why 100% PCI-CPB has a higher viscosity than Slag-CPBs. First, cement hydrates more quickly than slag does in the early stages. This causes more hydration products to form, like CH, ettringite, and C-S-H gel, which effectively bond the tailing particles together and raise the solid volume fraction and particle cohesion, both of which raise viscosity. Second, less hydration product production in the Slag-CPB suggests a smaller C-S-H gel-specific surface area, which reduces water adsorption and leaves more free water in the Slag-CPB. Particles are encased and lubricated by a water film created by this surplus-free water [33]. The case for the higher hydration product production in 100% PCI-CPB samples is experimentally supported by the findings of thermal analysis (TG/DTG) tests, which are used to determine the cement's phase stability and the amount of hydrates that are present. The XRD and TG/DTG diagrams for cement paste (CP) specimens containing Slag/PCI-CP and PCI-CP are shown in Figures 11 and 12, respectively. The TG/DTG curves for different CP combinations show that when the binder was made entirely of PCI, there was a noticeable increase in the presence of hydration products. Although this increased quantity is better for CPB hardening, it changes the flow capacity since C-S-H is the primary binding agent in cement-based products [11]. The results of monitoring the EC of CPB with 100% PCI and

with a mixture of PCI cement and slag (50/50), shown in Figure 13, experimentally validate the production of a higher number of cement hydration products in samples containing 100% PCI. This figure demonstrates that the sample with 100% PCI reached its maximum EC earlier than the sample with a cement blend, suggesting that the binder hydrated more quickly in the former scenario.



(**a**)



(**b**)

Figure 9. Effect of slag and nano-Al_2O_3 and binder type on the rheological properties of 2 h-old CPB. (**a**) Yield stress, (**b**) Viscosity.

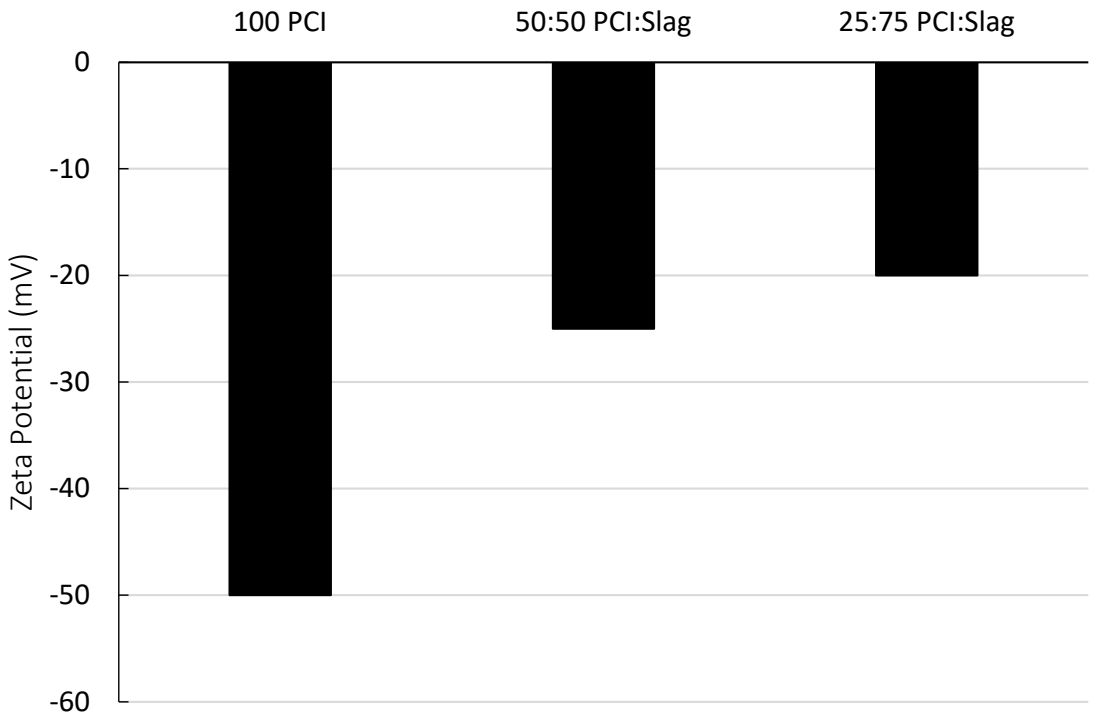


Figure 10. Zeta potentials of (100%) PCI-CPB vs. Slag-CPB (50:50 PCI: Slag) vs. Slag-CPB (25:75 PCI: Slag).

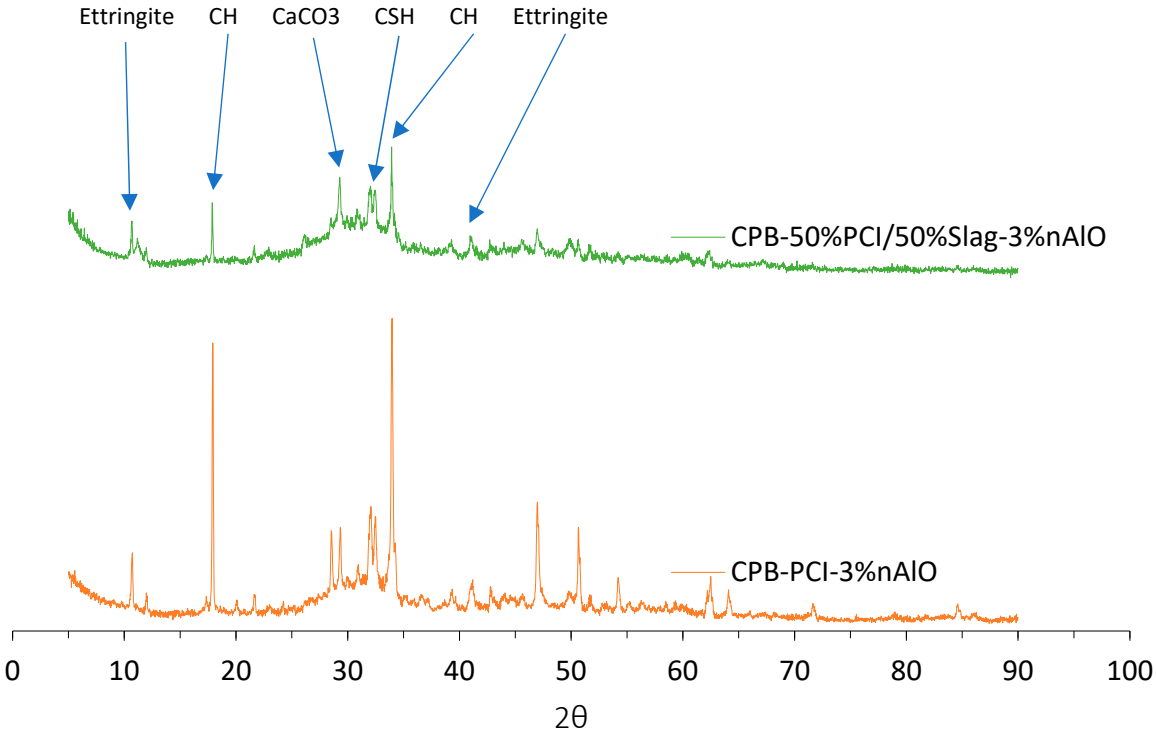


Figure 11. XRD results of cement paste of PCI/Slag (50/50), with the inclusion of 3%-nAlO samples after 2 h.

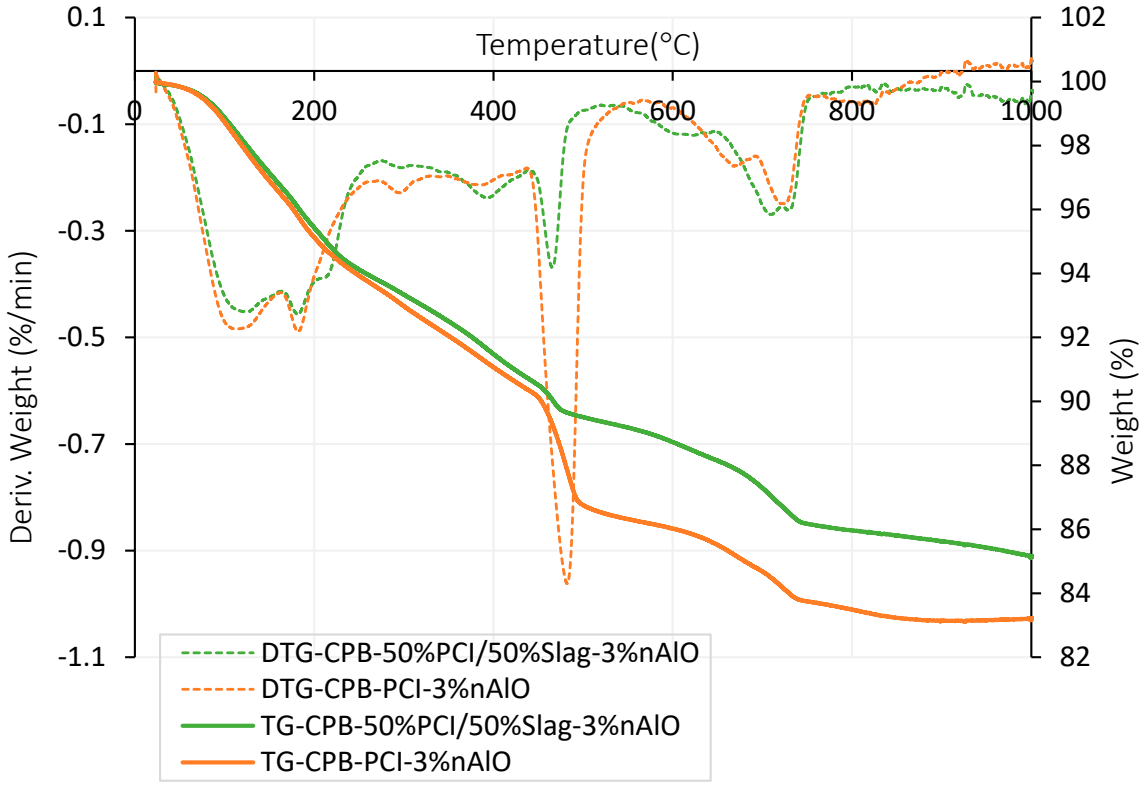


Figure 12. TG/DTG results of cement paste of PCI and PCI and PCI/Slag (50/50), with the inclusion of 3%-nAlO samples after 2 h.

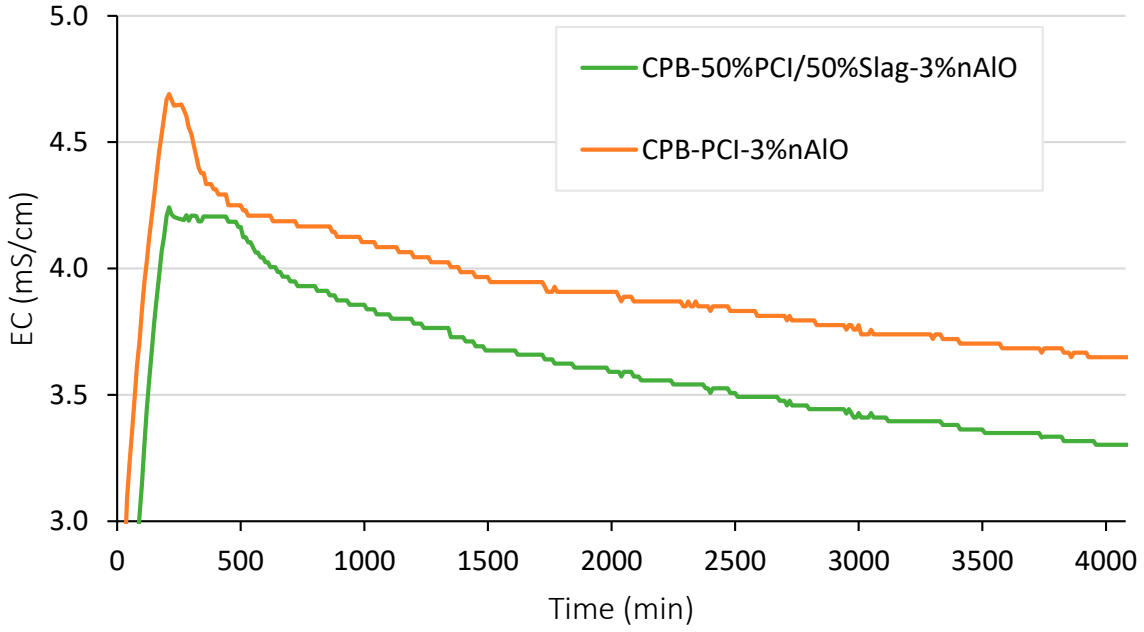


Figure 13. EC monitoring results of CPB samples with the PCI, PCI/Slag (50/50), with the inclusion of 3% nAlO.

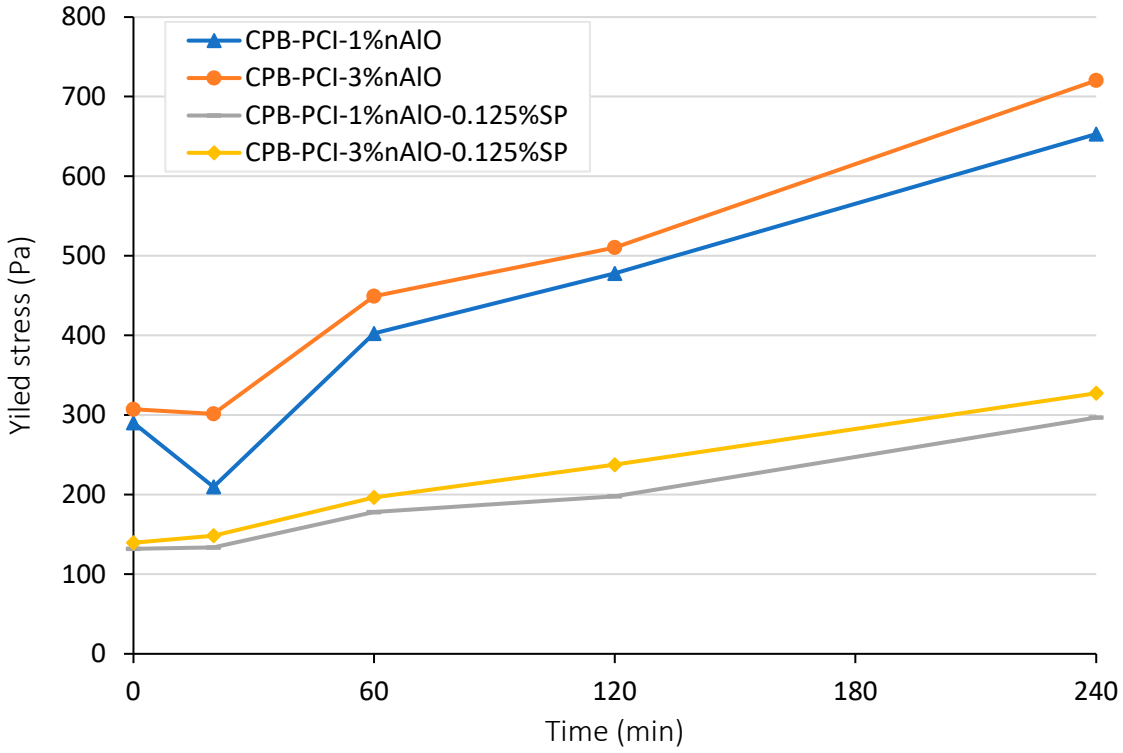
It is also clear from Figure 9 that adding nAlO raised the yield stress of all CPBs, regardless of the type of binder. Nevertheless, compared to PCI/Slag (50/50) and PCI-CPB samples, the yield stress of PCI/Slag (25/75) increased greater with increasing nAlO concentration. In fact, after two hours, the samples with PCI/Slag (25/75) had the highest yield stress at 3% nAlO (1064 Pa). The following interpretation can be made of this significant yield stress. First, when water is added to the mixture (pre-induction time),

some of the cement's ingredients, like gypsum and aluminate (C_3A), dissolve, and the solid concentration goes down a little [63,64]. Second, the Slag/PCI blended binder's early-age hydration processes progress more slowly than that of PCI alone, resulting in fewer hydration products and yield stress in the Slag-CPB mixture that is regulated by the first inter-particle forces [12]. Electrical conductivity monitoring studies, which show higher values in samples with higher Portland cement concentration, corroborate this slower hydration rate (Figure 13). On the other hand, delayed peak electrical conductivity is seen in CPBs with Slag/PCI blended binder, which suggests slower early-age hydration processes [65,66] (Figure 13). Because Portland cement hydration reduces the alkaline activating environment, the reactivity of CPB samples falls as the slag replacement % rises. Third, the mixture's negative zeta potential is raised by the consumption of calcium hydroxide (CH) via slag activation, improving flowability and repulsive force [67,68]. Furthermore, increased yield stress and viscosity of Slag-CPB are caused by increasing the amount of slag in the blended binder [65,69]. This is explained by the fact that slag particles have small particle sizes, which produce a filler effect that fills in gaps between cement particles and tailings grains, causing the backfill matrix to pack more densely [12,15]. Denser packing raises the friction coefficient between the particles, raising the yield stress. Furthermore, according to the Krieger-Dougherty model [63], denser packing raises the solid volume percentage and intensifies particle-particle interactions and viscosity.

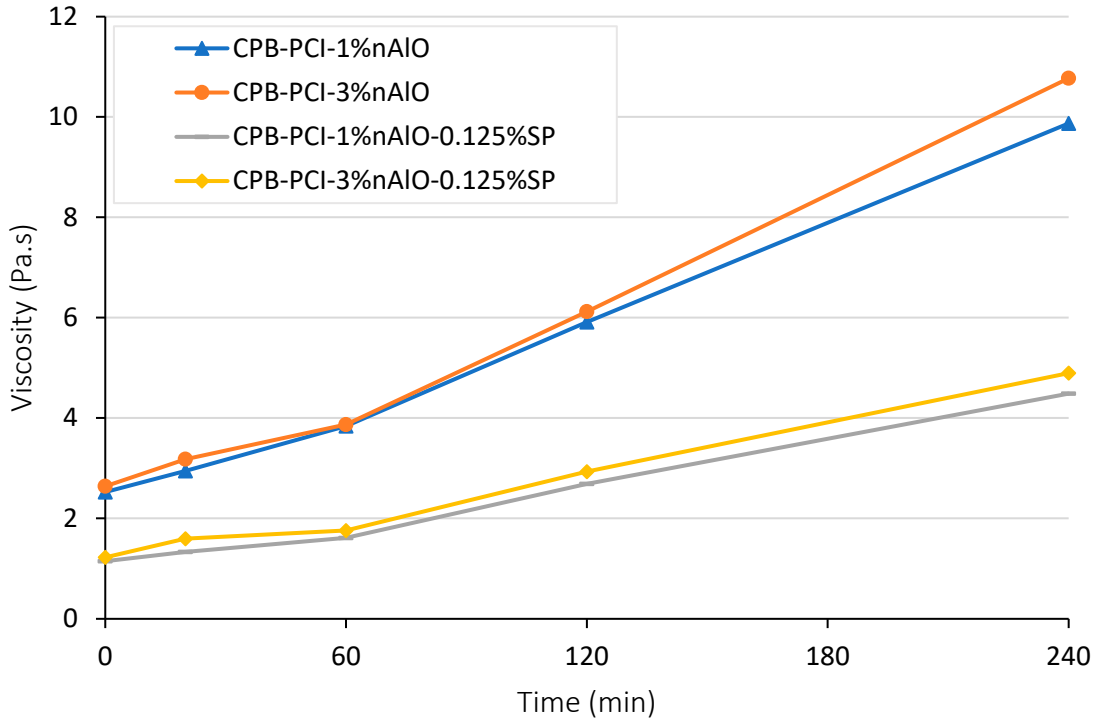
3.3. Impact of Superplasticizer on the Rheological Properties of CPB with nAlO

The results discussed above demonstrate that the inclusion of nAlO particles adversely affects the flow properties of CPB, potentially posing challenges for the efficient transport of newly modified CPBs containing nAlO particles in practical applications. This raises an important question: can the flow properties of CPB with nAlO be significantly improved through the addition of a superplasticizer? To address this, research was conducted to evaluate the influence of a superplasticizer on the rheological behaviour of CPB containing nAlO.

Figure 14 illustrates the effects of incorporating a superplasticizer (at 0.125% by weight of the mixture) on CPB samples with different nAlO concentrations. The yield stress (Figure 14a) and viscosity (Figure 14b) are shown for samples at various time intervals: 0, 20 min, 1 h, 2 h, and 4 h. This figure demonstrates that, regardless of the nanoparticle content, the addition of a superplasticizer significantly enhanced the flowability of CPB containing nAlO particles. For example, after 4 h of ageing, specimens with 3% and 1% nAlO exhibited reductions in yield stress of 53% and 54%, respectively, when treated with a superplasticizer. Similarly, a noticeable decrease in viscosity was observed. Moreover, Figure 14a indicates that CPB samples with higher nAlO content experienced a more pronounced reduction in yield stress due to the superplasticizer. This finding highlights the necessity of using a superplasticizer to effectively improve the flowability of CPB with higher nAlO concentrations. Enhancing the flowability of CPB with a superplasticizer not only improves pumping efficiency [70–76] but also reduces energy consumption and operating costs associated with transporting the underground nAlO-CPB material.



(**a**)



(**b**)

Figure 14. Effect of superplasticizer versus nano-Al_2O_3 on the evolution of CPB rheological properties. (**a**) Yield stress, (**b**) Viscosity.

The reduction in yield stress and viscosity observed with the addition of a superplasticizer can be attributed to the combination of two key factors. First, the dispersing effect of high-range water-reducing admixtures (WRAs) plays a significant role in this behaviour. Two different mechanisms of repulsion between cement particles are introduced by su-

perplasticizers derived from carboxylic compounds, like Master Glenium: (a) electrostatic repulsion due to the negative charges of the carboxylic group, and (b) steric repulsion due to the long polymer chains in the compound [36,66,72,73,77]. Second, the superplasticizer helps to delay the very early phases of cement hydration. Less hydration by-products are created when the repulsive force between the cement particles increases, which lowers the CPB's solid content and viscosity. TG/DTG diagrams of cement paste samples cured for two hours at different superplasticizer amounts, as shown in Figure 15, corroborate this conclusion. The diagrams show that in the cement paste without a superplasticizer, more hydration products are formed. More specifically, the sample with 0% superplasticizer shows the first peak at about 100–200 °C, which indicates the greatest weight loss. The development of products like gypsum, ettringite, and calcium-silicate-hydrate (C-S-H) is shown by the first peak (refs. [47,70–72,78–81]). Significantly fewer solid products are generated during the hydration process in the presence of the superplasticizer, according to the smaller peak shown in the TG/DTG data (Figure 15) of the cement paste sample. Furthermore, the findings of the EC monitoring shown in Figure 16 corroborate the claim that the superplasticizer slows down the hydration reaction. Higher ion mobility in the paste without the admixture is indicated by the electrical conductivity of the cement paste containing 0.125% superplasticizer being noticeably lower than that of the paste containing 0% superplasticizer. Furthermore, the superplasticizer-free sample exhibits a faster rate of cement hydration than the superplasticizer-containing sample, peaking at 210 min compared to 240 min for the latter.

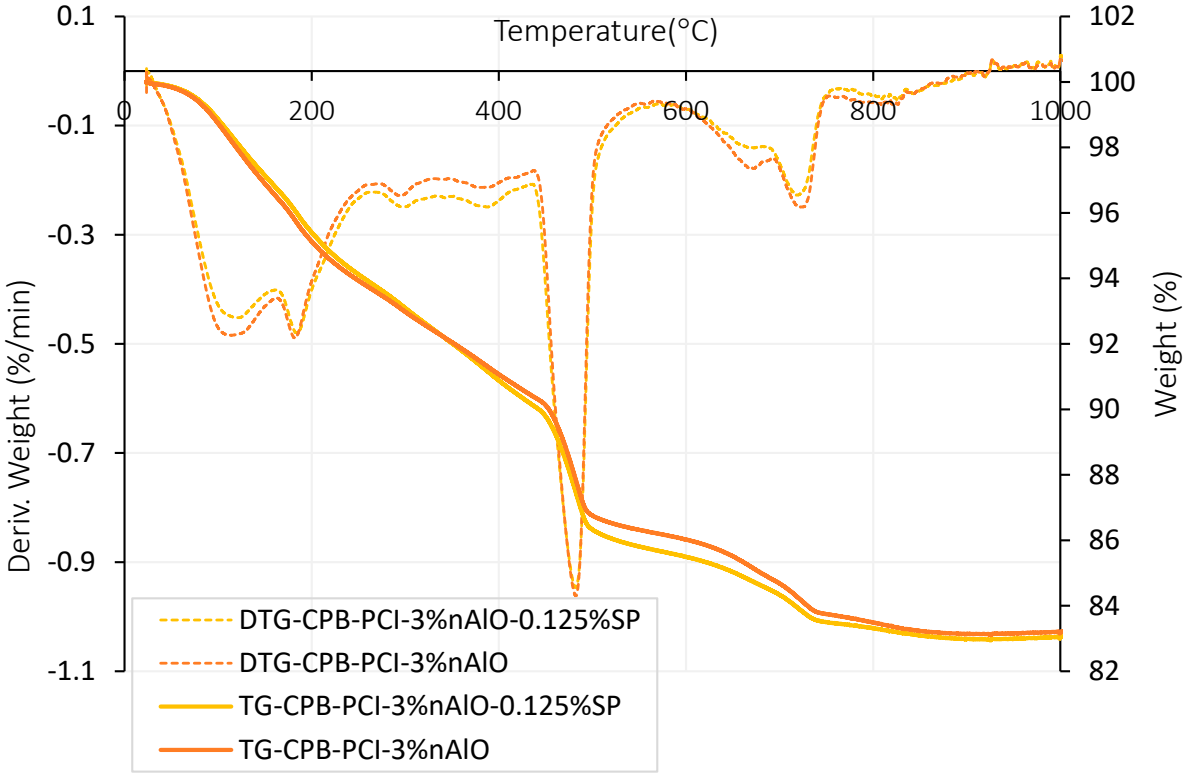


Figure 15. TG/DTG results of cement paste of PCI and PCI with the inclusion of 3% nAlO and 0.125% SP samples after 2 h.

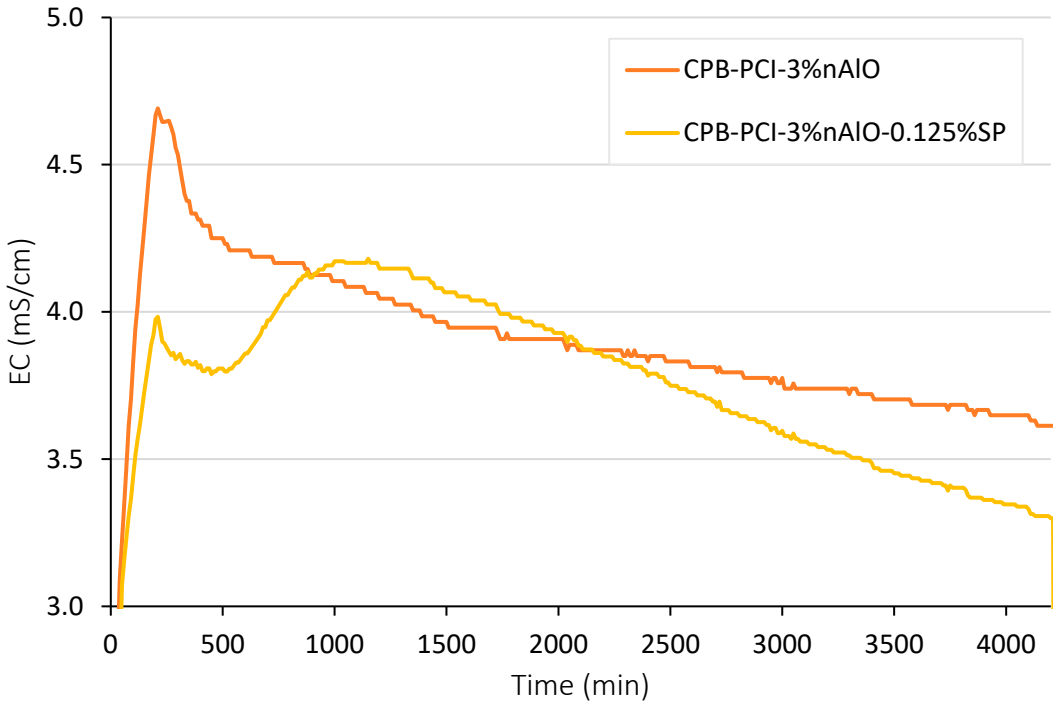


Figure 16. Displays the EC of the PCI with the inclusion of 3% nAlO and 0.125% SP.

4. Conclusions

The impact of nAlO on the rheological properties of cemented paste backfill (CPB) was examined experimentally in this study. Based on the findings, the following conclusions can be drawn:

- Adding nAlO particles or adjusting their dosage modifies CPB flowability by increasing yield stress and viscosity. This occurs due to (i) the filler effect of nAlO, (ii) its catalytic impact on cement hydration, (iii) increased water demand, and (iv) nAlO-induced flocculation or agglomeration of CPB particles.
- The influence of nAlO particles on rheology intensifies with longer curing or transport time due to increased hydration product formation and enhanced particle flocculation.
- The binder type in CPB preparation influences how nAlO affects flowability. As nAlO content increases, the yield stress of PCI-based CPB rises more gradually than in PCI/Slag (25/75) and PCI/Slag (50/50) samples. Thus, nAlO has a stronger impact on CPB with PCI/Slag binders over extended transport times. This is due to friction effects from multivalent cations between nAlO particles and the denser particle packing, which raises the solid volume fraction and enhances particle interactions, as explained by the Krieger–Dougherty model.
- Compared to PCI-CPB, Slag-CPB samples exhibited lower viscosity but higher yield stress. Higher binder concentration in Slag-CPB reduced both due to improved free water bleeding, despite the same water-to-cement ratio. However, increased Slag content reduced Slag-CPB flowability.
- Adding a superplasticizer to CPB with nAlO enhances flowability by increasing electrostatic repulsion between particles, with its effect becoming more pronounced at higher nAlO content.

Despite the results obtained, scaling up laboratory findings and conducting large-scale operations are essential to fully evaluate the cost-benefit ratio and practical applicability of nanoAlO-CPB technology. Moreover, future studies should investigate the reversibility of

structural buildup through re-shearing before each yield stress measurement of the yield stress of nAlO-CPB to gain a deeper understanding of its rheological behaviour.

Author Contributions: R.K.: Investigation, Writing – original draft. M.F.: Conceptualization, Methodology, Supervision, Resources, Project administration, Funding acquisition, Formal analysis, Writing – review & editing. All authors have read and agreed to the published version of the manuscript.

Funding: This research was funded by the Natural Sciences and Engineering Council of Canada (NSERC) and the University of Ottawa.

Data Availability Statement: The data presented in this study are available on request from the corresponding author.

Conflicts of Interest: The authors declare no conflict of interest.

References

1. Cui, L.; Fall, M. Multiphysics modeling and simulation of strength development and distribution in cemented tailings backfill structures. *Int. J. Concr. Struct. Mater.* **2018**, *12*, 25. [CrossRef]
2. Cui, L.; Fall, M. Multiphysics model for consolidation behavior of cemented paste backfill. *Int. J. Geomech.* **2017**, *17*, 04016077. [CrossRef]
3. Xu, W.; Zhang, Y.; Zuo, X.; Hong, M. Time-dependent rheological and mechanical properties of silica fume modified cemented tailings backfill in low temperature environment. *Cem. Concr. Compos.* **2020**, *114*, 103804. [CrossRef]
4. Bull, A.A.; Fall, M. Curing temperature dependency of the release of arsenic from cemented paste backfill made with Portland cement. *J. Environ. Manag.* **2020**, *269*, 110772. [CrossRef]
5. Qiu, J.; Guo, Z.; Yang, L.; Jiang, H.; Zhao, Y. Effects of packing density and water film thickness on the fluidity behaviour of cemented paste backfill. *Powder Technol.* **2020**, *359*, 27–35. [CrossRef]
6. Aldhafeeri, A.; Fall, M. Sulphate induced changes in the reactivity of cemented tailings backfill. *Int. J. Miner. Process.* **2017**, *166*, 13–23. [CrossRef]
7. Colangelo, F.; Forcina, A.; Farina, I.; Petrillo, A. Life Cycle Assessment (LCA) of Different Kinds of Concrete Containing Waste for Sustainable Construction. *Buildings* **2018**, *8*, 70. [CrossRef]
8. Fang, K.; Cui, L.; Fall, M. A coupled chemo-elastic cohesive zone model for backfill-rock interface. *Comput. Geotech.* **2020**, *125*, 103666. [CrossRef]
9. Al-Moselly, Z.; Fall, M.; Haruna, S. Further insight into the strength development of cemented paste backfill materials containing polycarboxylate ether-based superplasticizer. *J. Build. Eng.* **2022**, *47*, 103859. [CrossRef]
10. Simon, D.; Grabinsky, M. Apparent yield stress measurement in cemented paste backfill. *Int. J. Min. Reclam. Environ.* **2013**, *27*, 231–256. [CrossRef]
11. Taylor, H.F. *The Chemistry of Cements*; 1, 2. Print; Academic Press: London, UK, 1972.
12. Wu, D.; Fall, M.; Cai, S. Numerical modelling of thermally and hydraulically coupled processes in hydrating cemented tailings backfill columns. *Int. J. Min. Reclam. Environ.* **2014**, *28*, 173–199. [CrossRef]
13. Xiapeng, P.; Fall, M.; Haruna, S. Sulphate induced changes of rheological properties of cemented paste backfill. *Miner. Eng.* **2019**, *141*, 105849. [CrossRef]
14. Lavergne, F.; Belhadi, R.; Carriat, J.; Ben Fraj, A. Effect of nano-silica particles on the hydration, the rheology and the strength development of a blended cement paste. *Cem. Concr. Compos.* **2019**, *95*, 42–55. [CrossRef]
15. Zhang, M.H.; Islam, J. Use of nano-silica to reduce setting time and increase early strength of concretes with high volumes of fly ash or slag. *Constr. Build. Mater.* **2012**, *29*, 573–580. [CrossRef]
16. Justnes, H.; Vikan, H.V. Viscosity of Cement Slurries as a Function of Solids Content. 2005. Available online: https://api.semanticscholar.org/CorpusID:89612352 (accessed on 12 February 2024).
17. Bentz, D.P.; Ferraris, C.F.; Galler, M.A.; Hansen, A.S.; Guynn, J.M. Influence of particle size distributions on yield stress and viscosity of cement–fly ash pastes. *Cem. Concr. Res.* **2012**, *42*, 404–409. [CrossRef]
18. Li, Z.; Ohkubo, T.; Tanigawa, Y. Theoretical Analysis of Time-Dependence and Thixotropy of Fluidity for High Fluidity Concrete. *J. Mater. Civ. Eng.* **2004**, *16*, 247–256. [CrossRef]
19. Chin, C.-J.; Yiacoumi, S.; Tsouris, C. Probing DLVO Forces Using Interparticle Magnetic Forces: Transition from Secondary-Minimum to Primary-Minimum Aggregation. *Langmuir* **2001**, *17*, 6065–6071. [CrossRef]
20. Fornes, J.A. Secondary minimum analysis in the DLVO-theory. *Colloid Polym. Sci.* **1985**, *263*, 1004–1007. [CrossRef]
21. Chen, J.; Kou, S.; Poon, C. Hydration and properties of nano-TiO_2 blended cement composites. *Cem. Concr. Compos.* **2012**, *34*, 642–649. [CrossRef]

22. Land, G.; Stephan, D. The influence of nano-silica on the hydration of ordinary Portland cement. *J. Mater. Sci.* **2012**, *47*, 1011–1017. [CrossRef]
23. Li, Z.; Wang, H.; He, S.; Lu, Y.; Wang, M. Investigations on the preparation and mechanical properties of the nano-alumina reinforced cement composite. *Mater. Lett.* **2006**, *60*, 356–359. [CrossRef]
24. Oltulu, M.; Şahin, R. Pore structure analysis of hardened cement mortars containing silica fume and different nano-powders. *Constr. Build. Mater.* **2014**, *53*, 658–664. [CrossRef]
25. Quercia, G.; Spiesz, P.; Hüsken, G.; Brouwers, H.J.H. SCC modification by use of amorphous nano-silica. *Cem. Concr. Compos.* **2014**, *45*, 69–81. [CrossRef]
26. Said, A.M.; Zeidan, M.S.; Bassuoni, M.T.; Tian, Y. Properties of concrete incorporating nano-silica. *Constr. Build. Mater.* **2012**, *36*, 838–844. [CrossRef]
27. Senff, L.; Hotza, D.; Lucas, S.; Ferreira, V.M.; Labrincha, J.A. Effect of nano-SiO_2 and nano-TiO_2 addition on the rheological behavior and the hardened properties of cement mortars. *Mater. Sci. Eng. A* **2012**, *532*, 354–361. [CrossRef]
28. Zhang, M.; Li, H. Pore structure and chloride permeability of concrete containing nano-particles for pavement. *Constr. Build. Mater.* **2011**, *25*, 608–616. [CrossRef]
29. Bharathan, B.; McGuinness, M.; Kuhar, S.; Kermani, M.; Hassani, F.P.; Sasmito, A.P. Pressure loss and friction factor in non-Newtonian mine paste backfill: Modelling, loop test and mine field data. *Powder Technol.* **2019**, *344*, 443–453. [CrossRef]
30. Yang, L.; Yilmaz, E.; Li, J.; Liu, H.; Jiang, H. Effect of superplasticizer type and dosage on fluidity and strength behavior of cemented tailings backfill with different solid contents. *Constr. Build. Mater.* **2018**, *187*, 290–298. [CrossRef]
31. Wu, D.; Fall, M.; Cai, S.J. Coupling temperature, cement hydration and rheological behaviour of fresh cemented paste backfill. *Miner. Eng.* **2013**, *42*, 76–87. [CrossRef]
32. Yang, M. Interparticle Potential and Sedimentation Behavior of Cement Suspensions Review and Results from Paste. *Adv. Cem. Based Mater.* **1997**, *5*, 1–7. [CrossRef]
33. Yilmaz, E. Cemented coal fly ash backfill for mechanized underground coal mine application: Evaluating fresh and hardened properties. Keynote Address. In Proceedings of the 2024 International Conference on Green Intelligent Mining for Thick Coal Seam, Beijing, China, 22–24 November 2024.
34. Hanehara, S.; Yamada, K. Rheology and early age properties of cement systems. *Cem. Concr. Res.* **2008**, *38*, 175–195. [CrossRef]
35. *ASTM C494/C494M*; Standard Specification for Chemical Admixture for Concrete. ASTM International: West Conshohocken, PA, USA, 2004.
36. Haruna, S.; Fall, M. Time- and temperature-dependent rheological properties of cemented paste backfill that contains superplasticizer. *Powder Technol.* **2020**, *360*, 731–740. [CrossRef]
37. "Brookfield". Available online: https://pim-resources.coleparmer.com/instruction-manual/98945-xx.pdf (accessed on 14 January 2024).
38. *ASTM*; Standard Test Method for Laboratory Miniature Vane Shear Test for Saturated Fine-Grained Clayey Soil. American Society for Testing and Materials: West Conshohocken, PA, USA, 2016.
39. Clogston, J.D.; Patri, A.K. Zeta Potential Measurement. In *Characterization of Nanoparticles Intended for Drug Delivery*; McNeil, S.E., Ed.; Humana Press: Totowa, NJ, USA, 2011; pp. 63–70. [CrossRef]
40. Roshani, A.; Fall, M. Rheological properties of cemented paste backfill with nano-silica: Link to curing temperature. *Cem. Concr. Compos.* **2020**, *114*, 103785. [CrossRef]
41. Zhou, Y.; Fall, M.; Haruna, S. Flow ability of cemented paste backfill with chloride-free antifreeze additives in sub-zero environments. *Cem. Concr. Compos.* **2022**, *126*, 104359. [CrossRef]
42. Taylor, H.F. *Cement Chemistry*; Thomas Telford: London, UK, 1997; Volume 2.
43. American Society for Testing and Materials. *Cement, Concrete and Aggregates*; American Society for Testing and Materials: West Conshohocken, PA, USA, 1979.
44. Sha, W.; O'Neill, E.A.; Guo, Z. Differential scanning calorimetry study of ordinary Portland cement. *Cem. Concr. Res.* **1999**, *29*, 1487–1489. [CrossRef]
45. Sari, M.; Yilmaz, E.; Kasap, T. Long-term ageing characteristics of cemented paste backfill: Usability of sand as a partial substitute of hazardous tailings. *J. Clean. Prod.* **2023**, *401*, 136723. [CrossRef]
46. Pane, I.; Hansen, W. Investigation of blended cement hydration by isothermal calorimetry and thermal analysis. *Cem. Concr. Res.* **2005**, *35*, 1155–1164. [CrossRef]
47. Zhou, Q.; Glasser, F.P. Thermal stability and decomposition mechanisms of ettringite at< 120 C. *Cem. Concr. Res.* **2001**, *31*, 1333–1339.
48. Nonnet, E.; Lequeux, N.; Boch, P. Elastic properties of high alumina cement castables from room temperature to 1600 C. *J. Eur. Ceram. Soc.* **1999**, *19*, 1575–1583. [CrossRef]
49. Xiao, B.; Fall, M.; Roshani, A. Towards Understanding the Rheological Properties of Slag-Cemented Paste Backfill. *Int. J. Min. Reclam. Environ.* **2021**, *35*, 268–290. [CrossRef]

50. Zhou, Y.; Fall, M. Investigation on rheological properties of cemented pastefill with chloride-bearing antifreeze additives in sub-zero environments. *Cold Reg. Sci. Technol.* **2022**, *196*, 103506. [CrossRef]
51. Berkmen, Y.M.; Lande, A. Chest roentgenography as a window to the diagnosis of Takayasu's arteritis. *Am. J. Roentgenol.* **1975**, *125*, 842–846. [CrossRef] [PubMed]
52. Akbar, E.; Yaakob, Z.; Kamarudin, S.K.; Ismail, M.; Salimon, J. Characteristic and composition of Jatropha curcas oil seed from Malaysia and its potential as biodiesel feedstock feedstock. *Eur. J. Sci. Res.* **2009**, *29*, 396–403.
53. Cai, Y.; Hou, P.; Duan, C.; Zhang, R.; Zhou, Z.; Cheng, X.; Shah, S. The use of tetraethyl orthosilicate silane (TEOS) for surface-treatment of hardened cement-based materials: A comparison study with normal treatment agents. *Constr. Build. Mater.* **2016**, *117*, 144–151. [CrossRef]
54. Björnström, J.; Martinelli, A.; Matic, A.; Börjesson, L.; Panas, I. Accelerating effects of colloidal nano-silica for beneficial calcium–silicate–hydrate formation in cement. *Chem. Phys. Lett.* **2004**, *392*, 242–248. [CrossRef]
55. Sargam, Y.; Wang, K. Hydration kinetics and activation energy of cement pastes containing various nanoparticles. *Compos. Part B Eng.* **2021**, *216*, 108836. [CrossRef]
56. Carette, G.; Chevrier, A.B.R.L.; Malhotra, V.M. Mechanical Properties of Concrete Incorporating High Volumes of Fly Ash From Sources in the U.S. *Mater. J.* **1993**, *90*, 535–544. [CrossRef]
57. Roshani, A.; Fall, M. Flow ability of cemented pastefill material that contains nano-silica particles. *Powder Technol.* **2020**, *373*, 289–300. [CrossRef]
58. Wei, X. Study on hydration of Portland cement with fly ash using electrical measurement. *Mater. Struct.* **2005**, *38*, 411–417. [CrossRef]
59. McCarter, W.J.; Starrs, G.; Chrisp, T.M. Electrical conductivity, diffusion, and permeability of Portland cement-based mortars. *Cem. Concr. Res.* **2000**, *30*, 1395–1400. [CrossRef]
60. Madani, H.; Bagheri, A.; Parhizkar, T. The pozzolanic reactivity of monodispersed nanosilica hydrosols and their influence on the hydration characteristics of Portland cement. *Cem. Concr. Res.* **2012**, *42*, 1563–1570. [CrossRef]
61. Qing, Y.; Zenan, Z.; Deyu, K.; Rongshen, C. Influence of nano-SiO_2 addition on properties of hardened cement paste as compared with silica fume. *Constr. Build. Mater.* **2007**, *21*, 539–545. [CrossRef]
62. Fall, M.; Benzaazoua, M.; Ouellet, S. Experimental characterization of the influence of tailings fineness and density on the quality of cemented paste backfill. *Miner. Eng.* **2005**, *18*, 41–44. [CrossRef]
63. Krieger, I.M.; Dougherty, T.J. A Mechanism for Non-Newtonian Flow in Suspensions of Rigid Spheres. *Trans. Soc. Rheol.* **1959**, *3*, 137–152. [CrossRef]
64. Panchal, S.; Deb, D.; Sreenivas, T. Variability in rheology of cemented paste backfill with hydration age, binder and superplasticizer dosages. *Adv. Powder Technol.* **2018**, *29*, 2211–2220. [CrossRef]
65. Manmohan, D.; Mehta, P.K. Influence of pozzolanic, slag, and chemical admixtures on pore size distribution and permeability of hardened cement pastes. *Cem. Concr. Aggreg.* **1981**, *3*, 63–67. [CrossRef]
66. Topçu, İ.B.; Uygunoğlu, T.; Hocaoğlu, İ. Electrical conductivity of setting cement paste with different mineral admixtures. *Constr. Build. Mater.* **2012**, *28*, 414–420. [CrossRef]
67. Di, W.U.; Cai, S.; Huang, G. Coupled effect of cement hydration and temperature on rheological properties of fresh cemented tailings backfill slurry. *Trans. Nonferrous Met. Soc. China* **2014**, *24*, 2954–2963.
68. Deng, X.J.; Klein, B.; Zhang, J.X.; Hallbom, D.; De Wit, B. Time-dependent rheological behaviour of cemented backfill mixture. *Int. J. Min. Reclam. Environ.* **2018**, *32*, 145–162. [CrossRef]
69. Kocaba, V.; Gallucci, E.; Scrivener, K.L. Methods for determination of degree of reaction of slag in blended cement pastes. *Cem. Concr. Res.* **2012**, *42*, 511–525. [CrossRef]
70. Fall, M.; Célestin, J.C.; Pokharel, M.; Touré, M. A contribution to understanding the effects of curing temperature on the mechanical properties of mine cemented tailings backfill. *Eng. Geol.* **2010**, *114*, 397–413. [CrossRef]
71. Gomes, C.E.M.; Ferreira, O.P.; Fernandes, M.R. Influence of vinyl acetate-versatic vinylester copolymer on the microstructural characteristics of cement pastes. *Mater. Res.* **2005**, *8*, 51–56. [CrossRef]
72. He, X.F.; Miao, C.W.; Wu, Y.H.; Cao, X.X.; Liu, D. Thermal Reaction Kinetics of Fly Ash Cement Paste at the Age of 28 Days. *Appl. Mech. Mater.* **2014**, *668*, 91–94. [CrossRef]
73. Pereira, P.; Evangelista, L.; De Brito, J. The effect of superplasticisers on the workability and compressive strength of concrete made with fine recycled concrete aggregates. *Constr. Build. Mater.* **2012**, *28*, 722–729. [CrossRef]
74. Plank, J.; Vlad, D.; Brandl, A.; Chatziagorastou, P. Colloidal chemistry examination of the steric effect of polycarboxylate superplasticizers. *Cem. Int.* **2005**, *3*, 100–110.
75. Huynh, L.; Beattie, D.A.; Fornasiero, D.; Ralston, J. Effect of polyphosphate and naphthalene sulfonate formaldehyde condensate on the rheological properties of dewatered tailings and cemented paste backfill. *Miner. Eng.* **2006**, *19*, 28–36. [CrossRef]
76. Dhers, S.; Guggenberger, R.; Freimut, D.; Fataei, S.; Schwesig, P.; Martic, Z. Impact of Admixtures on Environmental Footprint, Rheological and Mechanical Properties of LC_3 Cemented Paste Backfill Systems. *Minerals* **2023**, *13*, 1552. [CrossRef]

77. Zhang, J.; Deng, H.; Taheri, A.; Deng, J.; Ke, B. Effects of Superplasticizer on the Hydration, Consistency, and Strength Development of Cemented Paste Backfill. *Minerals* **2018**, *8*, 381. [CrossRef]
78. Cavusoglu, I. Superplasticizer Dosage Effect on Strength, Microstructure and Permeability Enhancement of Cementitious Paste Fills. *Minerals* **2024**, *14*, 1242. [CrossRef]
79. Cavusoglu, I. Slag Substitution Effect on Features of Alkali-Free Accelerator-Reinforced Cemented Paste Backfill. *Minerals* **2025**, *15*, 135. [CrossRef]
80. Wang, Y.; Cao, Y.; Cao, C.; Wang, H. Effect of Curing Temperature under Deep Mining Conditions on the Mechanical Properties of Cemented Paste Backfill. *Minerals* **2023**, *13*, 383. [CrossRef]
81. Feng, Y.; Li, F.; Qi, W.; Ren, Q.; Qi, W.; Duan, G.; Zheng, K.; Han, Y.; Pang, H. Mechanical Properties and Microstructure of Iron Tailings Cemented Paste Backfills Using Carbide Slag-Activated Ground Granulated Blast-Furnace Slag as Alternative Binder. *Minerals* **2022**, *12*, 1549. [CrossRef]

Disclaimer/Publisher's Note: The statements, opinions and data contained in all publications are solely those of the individual author(s) and contributor(s) and not of MDPI and/or the editor(s). MDPI and/or the editor(s) disclaim responsibility for any injury to people or property resulting from any ideas, methods, instructions or products referred to in the content.